Journal of Medicinal Chemistry

Article

pubs.acs.org/jmc

9*H*-Purine Scaffold Reveals Induced-Fit Pocket Plasticity of the BRD9 Bromodomain

Sarah Picaud,[†,#] Maria Strocchia,[‡,#] Stefania Terracciano,[‡] Gianluigi Lauro,[‡] Jacqui Mendez,[§] Danette L. Daniels,[§] Raffaele Riccio,[‡] Giuseppe Bifulco,*[,‡] Ines Bruno,*[,‡] and Panagis Filippakopoulos*[,†,∥]

[†]Nuffield Department of Clinical Medicine, Structural Genomics Consortium, University of Oxford, Old Road Campus Research Building, Roosevelt Drive, Oxford OX3 7DQ, U.K.

[‡]Department of Pharmacy, University of Salerno, Via Giovanni Paolo II, 132, 84084 Fisciano, Italy

[§]Promega Corporation, 2800 Woods Hollow Road, Madison, Wisconsin 53711, United States

[∥]Nuffield Department of Clinical Medicine, Ludwig Cancer Research, University of Oxford, Old Road Campus Research Building, Roosevelt Drive, Oxford OX3 7DQ, U.K.

Supporting Information

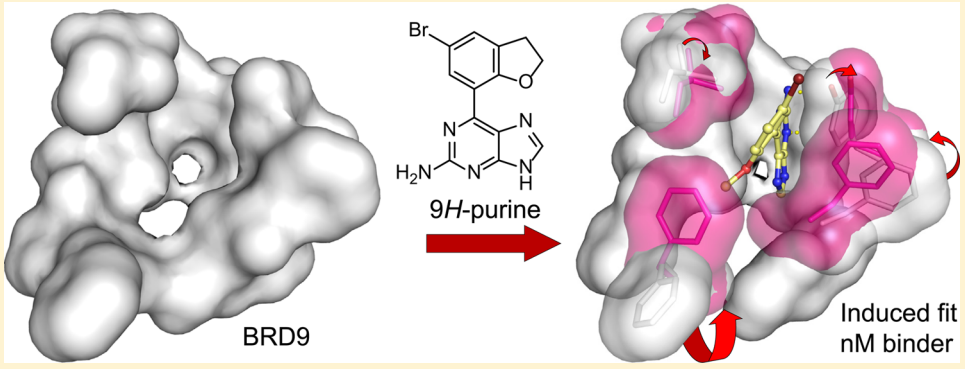

ABSTRACT: The 2-amine-9*H*-purine scaffold was identified as a weak bromodomain template and was developed via iterative structure based design into a potent nanomolar ligand for the bromodomain of human BRD9 with small residual micromolar affinity toward the bromodomain of BRD4. Binding of the lead compound **11** to the bromodomain of BRD9 results in an unprecedented rearrangement of residues forming the acetyllysine recognition site, affecting plasticity of the protein in an induced-fit pocket. The compound does not exhibit any cytotoxic effect in HEK293 cells and displaces the BRD9 bromodomain from chromatin in bioluminescence proximity assays without affecting the BRD4/histone complex. The 2-amine-9*H*-purine scaffold represents a novel template that can be further modified to yield highly potent and selective tool compounds to interrogate the biological role of BRD9 in diverse cellular systems.

INTRODUCTION

The term "epigenome" describes the array of chemical modifications on DNA and histone proteins that dynamically regulate gene expression.[1] The complex set of reversible post-translational modifications (PTMs) that decorate histones ultimately determines the overall state of chromatin, giving rise to the so-called "histone code", a cellular language involving specific proteins that introduce (writers), remove (erasers), or recognize (readers) PTMs.[2] ε-N-acetylation of lysine residues is a widespread post-translational mark,[3] deposited on proteins throughout the entire proteome by lysine acetyl transferases (KATs), removed by lysine deacetylases (KDACs), and recognized by evolutionary conserved protein modules such as bromodomains[4] (named after the *Drosophila melanogaster brahma* gene[5]) as well as the more recently discovered YEATS domains.[6] The human proteome encodes 61 bromodomains (BRDs) found on 42 diverse proteins, including histone acetyl transferases (HATs) and HAT-associated proteins such as GCN5, PCAF, and bromodomain 9 (BRD9),[7,8] transcriptional coactivators such as the TAF and TRIM/TIF proteins,[9,10] ATP-dependent chromatin remodeling complexes such as BAZ1B,[11] helicases such as SMARCA,[12] nuclear scaffolding proteins such as the polybromo PB1[13] as well as transcriptional regulators, such as the bromo and extra terminal (BET) proteins.[14] The family of human BRD modules has almost been completely structurally characterized resulting in a recent classification of eight distinct structural subfamilies.[15]

The BET subfamily of BRDs has attracted a lot of attention, as its members (BRD2, BRD3, BRD4, and the testis specific BRDT) play a central role in cell cycle progression, cellular proliferation, and apoptosis.[16] BETs contain two N-terminal

Received: December 5, 2014
Published: February 22, 2015

DOI: 10.1021/jm501893k
J. Med. Chem. 2015, 58, 2718−2736

Chart 1. Acetyllysine Mimetic Templates Reported To Bind to Bromodomain Proteins[a]

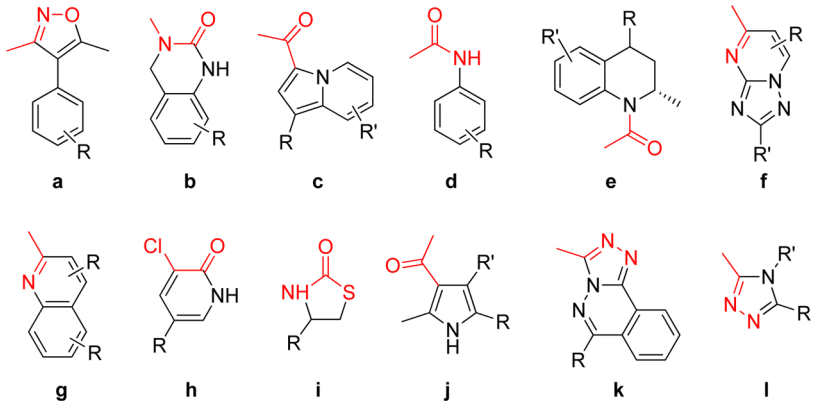

[a]The Kac mimetic portion of each substructure is highlighted in red. (a) 3,4-Dimethylisoxazole; (b) 3-methyl-3,4-dihydroquinazolinone; (c) indolizinethanone; (d) *N*-phenylacetamide; (e) *N*-acetyl-2-methyltetrahydroquinoline; (f) triazolopyrimidine; (g) methylquinoline; (h) chloropyridone; (i) thiazolidinone; (j) 4-acylpyrrole; (k) triazolophtalazine; (l) methyltriazoles.

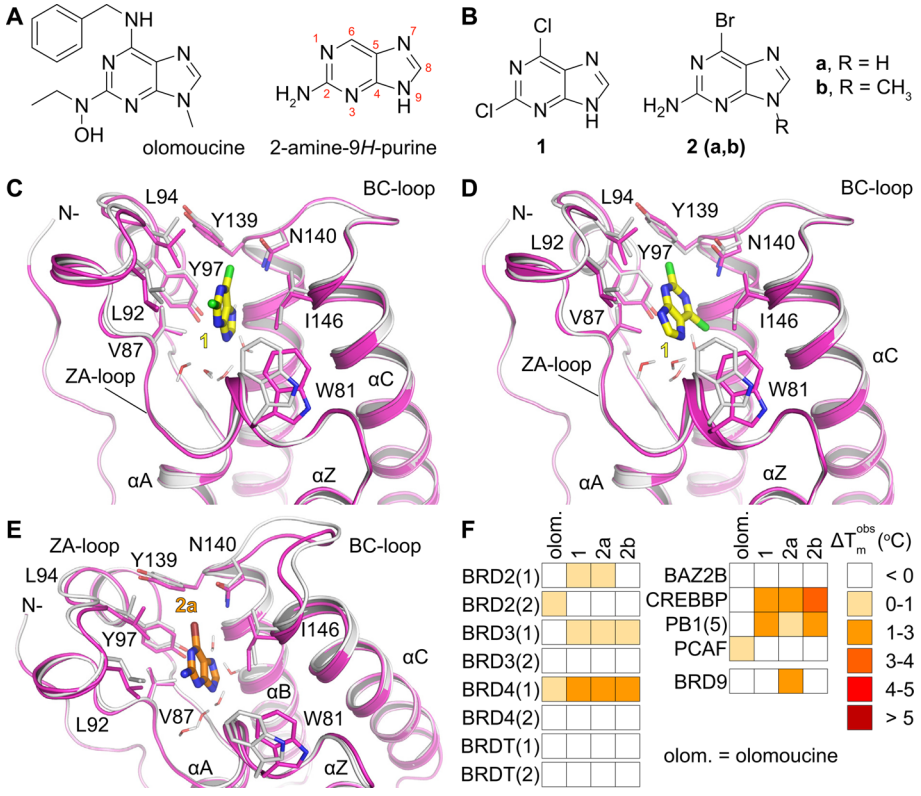

Figure 1. Purine fragments bind to human bromodomains. (A) Structure of olomoucine, a potent cyclin-dependent kinase inhibitor and numbering of the 2-amine-9*H*-purine core scaffold. (B) Purine fragments tested as bromodomain ligands. (C) Docking pose of **1** (yellow stick representation) onto the bromodomain of BRD4(1) positions the bulky halogen group on the top of the binding pocket. The protein is shown as a white ribbon (starting model, PDB code 4MEN) or in magenta (docked model) with characteristic residues shown as sticks in the same color scheme. (D) Alternative binding of compound **1** into the bromodomain of BRD4(1) with the 6-chloro substituent adopting an acetyllysine mimetic pose. The compound and protein are colored as in (C). PDB code 4MEN was used as the starting model for docking. (E) Docking of compound **2a** positions the 2-amine-9*H*-purine ring system of the ligand within the Kac cavity, sterically packing between V87 and I146, suggesting that this scaffold topology can be further utilized to target bromodomains. The same color scheme as in (C) and (D) is used with the ligand shown as orange sticks. PDB code 4MEN was used as the starting model for docking. (F) Fragments were tested in a thermal shift assay against bromodomains of the BET subfamily as well as representative members from other families. Thermal shifts are color-coded as indicated in the inset. 9*H*-Purines showed weak binding across the panel.

BRD modules that interact with acetylated histones,[15] transcription factors[17,18] or other acetylated transcriptional regulators,[19,20] an extra terminal (ET) recruitment domain,[21] and a C-terminal motif (in the case of BRD4 and BRDT) responsible for the recruitment of the positive transcription elongation factor B (P-TEFb),[22] ultimately controlling transcriptional elongation. Importantly, BET BRDs have been successfully targeted by small molecule inhibitors, such as the triazolothienodiazepine (+)-JQ1[23] and the triazolobenzodiazepine IBET762,[24] which were identified employing phenotypic

DOI: 10.1021/jm501893k
J. Med. Chem. 2015, 58, 2718−2736

Chart 2. Chemical Structures of Compounds 1−11

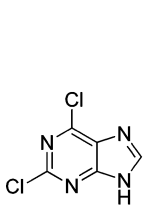

1

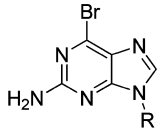

2 (a,b)

a, R=H
b, R=CH_3

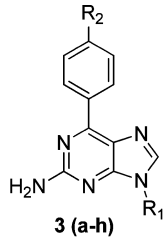

3 (a-h)

a, R_1 = H, R_2 = H
b, R_1 = H, R_2 = OCH_3
c, R_1 = CH_3, R_2 = OCH_3
d, R_1 = H, R_2 = OPh
e, R_1 = CH_3, R_2 = OPh
f, R_1 = H, R_2 = OCH_2Ph
g, R_1 = H, R_2 = CH_2O-m-$PhCF_3$
h, R_1 = H, R_2 = CH_2O-p-$PhCH_2CH_2OCH_3$

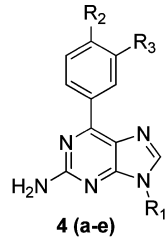

4 (a-e)

a, R_1 = H, R_2 = OCH_2Ph, R_3 = Cl
b, R_1 = H, R_2 = OCH_2-m,m'-$Ph(OCH_3)_2$, R_3 = Cl
c, R_1 = H, $R_{2,3}$ = -OCH_2CH_2O-
d, R_1 = H, R_2 = H, R_3 = OCH_2-p-PhCl
e, R_1 = CH_3, R_2 = H, R_3 = OCH_2-p-PhCl

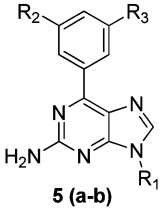

5 (a-b)

a, R_1 = H, R_2 = Br, R_3 = $O(CH_2)_3CH_3$
b, R_1 = CH_3, R_2 = Br, R_3 = $O(CH_2)_3CH_3$

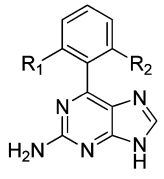

6 (a-c)

a, R_1 = OCH_3, R_2 = OCH_3
b, R_1 = OCH_3, R_2 = $OCH(CH_3)_2$
c, R_1 = OCH_3, R_2 = $OCH_2CH(CH_3)_2$

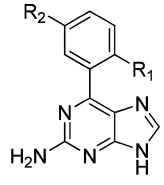

7 (a-e)

a, R_1 = OCH_3, R_2 = H
b, R_1 = OCH_3, R_2 = F
c, R_1 = OCH_3, R_2 = Cl
d, R_1 = OCH_3, R_2 = Br
e, R_1 = OCH_2CH_3, R_2 = Br

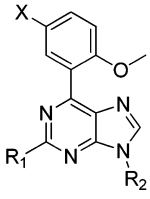

8 (a-f)

a, X = Br, R_1 = Cl, R_2 = H
b, X = Br, R_1 = NH_2, R_2 = CH_3
c, X = Br, R_1 = NH_2, R_2 = $CH_2(C=O)CH_3$
d, X = F, R_1 = OH, R_2 = H
e, X = Cl, R_1 = OH, R_2 = H
f, X = Br, R_1 = OH, R_2 = H

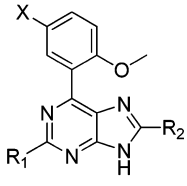

9 (a-b)

a, X = Br, R_1 = H, R_2 = CH_3
b, X = F, R_1 = H, R_2 = CH_3

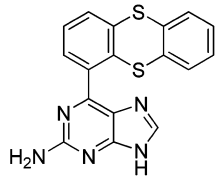

10

11

screening and have in the past few years consolidated the emerging role of BRDs as viable therapeutic targets. Indeed, BET inhibition suppresses tumor growth in diverse mouse models of cancer, such as NUT midline carcinoma, acute myeloid and mixed lineage leukemia, multiple myeloma, glioblastoma, melanoma, Burkitt's lymphoma, neuroblastoma and prostate cancer, leading to a number of clinical trials seeking to modulate BET function in diverse tumor settings.[25]

The initial success targeting BET proteins and the availability of robust recombinant systems of expression as well as biophysical assays to probe BET−ligand interactions have spawned a number of medicinal chemistry efforts seeking to identify novel scaffolds that can block binding of acetylated lysines to these protein interaction modules. Phenotypic screening, molecular docking, and fragment-based approaches have emerged as successful tools for discovering other Kac mimetics, leading to the identification of a number of new chemotypes, including 3,4-dimethylisoxazoles,[26,27] 3-methyl-3,4-dihydroquinazolinones,[28] indolizinethanones, *N*-phenylacetamides, and *N*-acety-2-methyltetrahydroquinolines[29] triazolopyrimidines, methylquinoline, and chloropyridones,[30] thiazolidinones,[31] 4-acylpyrroles,[32] and triazolophtalazines[33] (summerized in Chart 1). Starting from fragment hits, highly potent and selective BET inhibitors have also emerged,[34,35] suggesting that it is possible to access new chemical space for inhibitor development via initial fragment screening. Druggability analysis based on the available structural information[36] suggests that it is possible to target most BRD structural classes.[15] In fact, BRDs annotated as "hard" to target, such as BAZ2B, have recently been successfully targeted by highly selective and potent inhibitors[37] and fragment based approaches have now yielded chemotypes targeting BRDs outside the BET family, including CREBBP/p300,[38] ATAD2,[39,40] BAZ2B,[41] and BRPF1.[42]

DOI: 10.1021/jm501893k
J. Med. Chem. 2015, 58, 2718−2736

An unexpected but interesting finding that recently attracted attention was the identification of clinically approved kinase inhibitors and tool compounds that exhibited binding with high affinity, and selectivity across the human BRD family, to BET BRDs.[43] Crystal structures with the first bromodomain of BRD4 revealed acetyllysine mimetic binding of the PLK inhibitor BI-2536 and the JAK inhibitor fedratinib without any significant distortion of the inhibitors when compared to kinase complexes, suggesting the potential to develop polypharmacology targeting both BRD and kinases at the same time.[43] Interestingly, the cyclin-dependent kinase inhibitor dinaciclib was also identified as a binder of BRD4,[44] suggesting that other inhibitor classes might be good starting points for developing inhibitors for BRDs.

In light of the successful fragment-based programs and the reliability for discovering BRDs inhibitors, we started to investigate the purine scaffold as a putative Kac mimetic. Purine is a privileged chemical template, as it is one of the most abundant N-based heterocycles in nature,[45] and a number of purine-based drugs are currently approved and used for the treatment of cancer (6-mercaptopurine, 6-thioguanine), viral infections such as AIDS and herpes (carbovir, abacavir, acyclovir, ganciclovir), hairy cell leukemia (cladribine), and organ rejection (azathioprine).[46] Moreover, purine based compounds have emerged as reliable chemical−biology tools, since they can interact with a variety of biological targets involved in a number of diseases. Some such examples include their activity as microtubule (myoseverin), 90-heat shock protein (PU3), sulfotransferase (NG38), adenosine receptor (KW-6002), and cyclin-dependent kinase (olomoucine, Figure 1A; roscovitine) inhibitors.[47,48]

Computational analyses followed by in vitro evaluation of purine-based fragments identified this scaffold as a novel effective Kac mimetic. Interestingly, initial purine fragment hits also demonstrated affinity outside the BET subfamily of BRDs, toward the less explored BRDs of PB1, CREBBP, and BRD9. To our knowledge, the only known BRD9 inhibitors today show cross-reactivity toward BET BRDs and CREBBP employing a triazolophthalazine template.[33] The precise biological function of BRD9 remains elusive, although it has been identified as a component of the SWI/SNF complex[49] and has been associated with a number of different cancer types, including non-small-cell lung cancer,[50] cervical,[51] and hepatocellular carcinoma.[52] Notably, its BRD reader module has been frequently found mutated in lung squamous cell carcinoma, prostate adenocarcinoma, and uterine corpus endometrial carcinoma.[53−55]

We chose a small purine fragment, compound **2a** (Chart 2), from our fragment hits for structural optimization and found that some of its 6-aryl derivatives exhibited nanomolar affinity toward BRD9, with lower activity toward BRD4. Importantly, the developed inhibitors induced an appreciable change in the three-dimensional shape of the receptor binding cavity, indicating that their binding occurs through an "induced-fit" mechanism.[56] Previously an induced fit binding was observed when a dihydroquinoxalinone was shown to insert under an arginine residue of the CREBBP BRD, resulting in restructuring of the Kac binding site of this bromodomain.[57] In our case the rearrangement of the binding site of BRD9 was more extensive, with several side chains rotating and shifting to accommodate the small purine ligand. The optimized compound **11** (Chart 2) exhibited nanomolar affinity for BRD9 with weaker micromolar affinity for BRD4 in vitro, displaced the BRD9 BRD from chromatin without affecting BRD4 binding to histones, and did not show any cytotoxicity toward human embryonic kidney cells. Our work establishes the proof-of-concept of using 2-amino-9*H*-purines as a starting point to develop Kac mimetic compounds targeting BRDs outside the BET family, with compound **11** representing a promising low nanomolar starting point toward the discovery of selective BRD9 ligands to be used as chemical probes for deep biological and pharmacological investigation of BRD9.

EXPERIMENTAL DETAILS

Input Files Preparation for Docking. Protein 3D models of BRD4 (first bromodomain, PDB code 4MEN[30]) and BRD9 (apo form, PDB code 3HME[15]) were prepared using the Schrödinger Protein Preparation Wizard workflow (Schrödinger, LLC, New York, NY, 2013). Briefly, water molecules that were found 5 Å or more away from heteroatom groups were removed and cap termini were included. Additionally, all hydrogen atoms were added, and bond orders were assigned. The resulting PDB files were converted to the MAE format. Chemical structures of investigated compounds were built with Maestro's Build Panel (version 9.6; Schrödinger, LLC, New York, NY, 2013) and subsequently processed with LigPrep (version 2.8; Schrödinger, LLC, New York, NY, 2013) in order to generate all the possible stereoisomers, tautomers, and protonation states at a pH of 7.4 ± 1.0; the resulting ligands were finally minimized employing the OPLS 2005 force field.

Induced Fit Docking. Binding sites for the initial Glide[58−60] (version 6.1, Schrödinger, LLC, New York, NY, 2013) docking phases of the Induced Fit Workflow (Induced Fit Docking protocol 2013-3, Glide version 6.1, Prime version 3.4, Schrödinger, LLC, New York, NY, 2013)[61,62] were calculated on the BRD4(1) and BRD9 structures, considering the centroid of the cocrystallized ligand (*N*,5-dimethyl-*N*-(4-methylbenzyl)[1,2,4]triazolo[1,5-*a*]pyrimidin-7-amine for BRD4(1), from PDB code 4MEN), or cocrystallized ligand **7d** (from the BRD9/**7d** complex), or Tyr106 (for BRD9, PDB code 3HME) for grid generation. In all cases, cubic inner boxes with dimensions of 10 Å were applied to the proteins, and outer boxes were automatically detected. Ring conformations of the investigated compounds were sampled using an energy window of 2.5 kcal/mol; conformations featuring nonplanar conformations of amide bonds were penalized. Side chains of residues close to the docking outputs (within 8.0 Å of ligand poses) were reoriented using Prime (version 3.4, Schrödinger, LLC, New York, NY, 2013), and ligands were redocked into their corresponding low energy protein structures (Glide Standard Precision Mode), considering inner boxes dimensions of 5.0 Å (outer boxes automatically detected), with resulting complexes ranked according to GlideScore.

Rigid Docking. Calculations were performed using the Glide software package (SP mode, version 6.1, Schrödinger package)[58−60] in order to determine the binding mode of compound **11** into the acetyllysine cavity of BRD9. First the receptor grid was generated focused on the BRD9 binding site taking as a reference structure the experimentally determined complex structure of compound **7d** with BRD9, with inner- and outer-box dimensions of 10 × 10 × 10 and 21.71 × 21.71 × 21.71, respectively. Standard Precision (SP) Glide mode was employed accounting for compound flexibility in the sampling of compound **11**. The sampling step was set to expanded sampling mode (4 times), keeping 10 000 ligand poses for the initial phase of docking, followed by 800 ligand poses selection for energy minimization. A maximum number of 50 output structures were saved for each ligand, with a scaling factor of 0.8 related to van der Waals radii with a partial charge cutoff of 0.15. A postdocking optimization of the obtained docking outputs was performed, accounting for a maximum of 50 poses based on a 0.5 kcal/mol rejection cutoff for the obtained minimized poses.

General Synthetic Information. All commercially available starting materials were purchased from Sigma-Aldrich and were used as received. Solvents used for the synthesis were of HPLC grade and

DOI: 10.1021/jm501893k
J. Med. Chem. 2015, 58, 2718−2736

were purchased from Sigma-Aldrich or Carlo Erba Reagenti. NMR spectra were recorded on Bruker Avance 600 or 300 MHz instruments. Compounds were dissolved in 0.5 mL of MeOD, $CDCl_3$, or DMSO-d_6. Coupling constants (J) are reported in hertz, and chemical shifts are expressed in parts per million (ppm) on the δ scale relative to the solvent peak as internal reference. ^{13}C spectra are reported for representative compounds. Electrospray mass spectrometry (ESI-MS) was performed on a LCQ DECA TermoQuest (San Jose, CA, USA) mass spectrometer. Chemical reactions were monitored on silica gel 60 F_{254} plates (Merck), and spots were visualized under UV light. Analytical and semipreparative reversed-phase HPLC were performed on an Agilent Technologies 1200 series high performance liquid chromatography system using Jupiter Proteo C_{18} reversed-phase columns ((a) 250 mm × 4.60 mm, 4 μm, 90 Å, flow rate = 1 mL/min; (b) 250 mm × 10.00 mm, 10 μm, 90 Å, flow rate = 4 mL/min respectively, Phenomenex). The binary solvent system (A/B) was as follows: 0.1% TFA in water (A) and 0.1% TFA in CH_3CN (B). Absorbance was detected at 240 nm. The purity of all tested compound (>98%) was determined by HPLC analysis. Microwave irradiation reactions were carried out in a dedicated CEM-Discover focused microwave synthesis apparatus, operating with continuous irradiation power from 0 to 300 W utilizing the standard absorbance level of 300 W maximum power. Reactions were carried out in 10 mL sealed microwave glass vials. The Discover system also included controllable ramp time, hold time (reaction time), and uniform stirring. After the irradiation period, reaction vessels were cooled rapidly (60−120 s) to ambient temperature by air jet cooling. Compounds synthesized are shown in Chart 2.

General Procedure *a* for the Suzuki−Miyaura Cross-Coupling of Free Halopurines (3a,b, 3d, 3f−h, 4a−d, 5a, 6a−c, 7a−e, 8a, 9a,b, 10, 11). 2-Amino-6-bromopurine (50.0 mg, 0.23 mmol), commercially available boronic acids (0.29 mmol), $Pd(OAc)_2$ (2.70 mg, 0.012 mmol), $P(C_6H_4SO_3Na)_3$ (34.0 mg, 0.06 mmol), and Cs_2CO_3 (228.0 mg, 0.70 mmol) were added to a 10 mL microwave vial equipped with a magnetic stirrer. The vial was evacuated and backfilled with nitrogen three times. Degassed acetonitrile (0.5 mL) and degassed water (1.0 mL) were added by means of an airtight syringe. The mixture was heated under microwave irradiation at 150 °C for 5−15 min. After irradiation, the vial was cooled to ambient temperature by air jet cooling and a mixture of cold water and HCl (1.5 M) was added (5.0 and 2.0 mL, respectively). The mixture was subsequently poured into crushed ice and then left at 4 °C overnight. The resulting precipitate was filtered and purified by HPLC to give the desired product in good yields (53−90%). HPLC purification was performed by semipreparative reversed-phase HPLC using the gradient conditions reported below for each compound. The final products were obtained with high purity (>95%) detected by HPLC analysis and were fully characterized by ESI-MS and NMR spectroscopy.

General Procedure *b* for TBAF-Assisted N9-Alkylation of Purine Rings (2b, 3c, 3e, 4e, 5b, 8b, 8c). 2-Amino-6-arylpurine (0.1 mmol) was dissolved in 0.4 mL of THF at room temperature. To this mixture 0.2 mL (0.2 mmol) of TBAF (1.0 M solution in THF, Aldrich) and iodomethane (12.5 μL, 0.2 mmol) or chloroacetone (16.0 μL, 0.2 mmol) were added. The reaction was stirred at room temperature for 10 min. Water was added, and the aqueous layer was extracted three times with dichloromethane. The combined organic layers were washed with water, dried with anhydrous Na_2SO_4 and concentrated under vacuum. The crude mixture was purified by semipreparative reversed-phase HPLC using the gradient conditions reported below for each compound. Compounds were obtained in good yields (50−88%) and high purity (>98%) and were fully characterized by ESI-MS and NMR spectroscopy.

General Procedure *c* for the Synthesis of 2-Hydroxyl-6-arylpurines (8d−f). A three-necked flask was charged with the 2-amino-6-arylpurine derivative (**7b−d**) (0.5 mmol) and 50% H_2SO_4 (2.0 mL). The mixture was stirred at room temperature for 30 min and then cooled to −5 °C. A solution of $NaNO_2$ (48.3 mg, 0.7 mmol) in H_2O (200 μL) was added dropwise, and the release of nitrogen gas was immediately observed. The reaction mixture was then stirred at −10 °C for 2 h, and urea (24.0 mg, 0.4 mmol) was added to decompose the excess of $NaNO_2$. The mixture was then stirred at 50 °C for 1 h and neutralized with 50% NaOH solution, diluted with water, and extracted three times with EtOAc. The combined organic layers were dried with anhydrous Na_2SO_4 and concentrated under vacuum. The crude mixture was purified by semipreparative reversed-phase HPLC to get the pure products in good yields (47−63%). Compounds were fully characterized by ESI-MS and NMR spectroscopy.

2-Amino-6-bromo-9-methylpurine (2b). **2b** was obtained from commercially available **2a** following general procedure *b* as a yellow powder in 85% yield. RP-HPLC: t_R = 12.4 min, gradient condition from 5% B to 100% B in 95 min, flow rate of 4 mL/min, λ = 240 nm. ^1H NMR (600 MHz, MeOD): δ = 3.74 (s, 3H), 8.25 (s, 1H). ^{13}C NMR (150 MHz, MeOD): δ = 30.6, 126.3, 142.5, 149.4, 155.62, 160.8. ESI-MS, calculated for $C_6H_6BrN_5$ 227.0; found m/z = 228.1 $[M + H]^+$.

2-Amino-6-phenyl-9*H*-purine (3a). **3a** was obtained following general procedure *a* as a white powder in 90% yield from **2a** and phenylboronic acid **13**. RP-HPLC t_R = 12.1 min, gradient condition from 5% B to 100% B in 60 min, flow rate of 4 mL/min, λ = 240 nm. Spectral data were in accord with previously published data.[63]

2-Amino-6-(4-methoxyphenyl)-9*H*-purine (3b). **3b** was obtained following general procedure *a* as a pale yellow powder in 86% yield from **2a** and 4-methoxyphenylboronic acid **14**. RP-HPLC t_R = 14.6 min, gradient condition from 5% B to 100% B in 65 min, flow rate of 4 mL/min, λ = 240 nm. Spectral data were in accord with previously published data.[64]

2-Amino-6-(4-methoxyphenyl)-9-methylpurine (3c). **3c** was obtained following general procedure *b* as a yellow powder in 88% yield from **3b**. RP-HPLC t_R = 15.5 min, gradient condition from 5% B to 100% B in 65 min, flow rate of 4 mL/min, λ = 240 nm. ^1H NMR (300 MHz, $CDCl_3$): δ = 3.79 (s, 3H), 3.94 (s, 3H), 7.12 (d, J = 8.6 Hz, 2H), 7.95 (s, 1H), 8.55 (d, J = 8.5 Hz, 2H). ESI-MS, calculated for $C_{13}H_{13}N_5O$ 255.1; found m/z = 256.3 $[M + H]^+$.

2-Amino-6-(4-phenoxyphenyl)-9*H*-purine (3d). **3d** was obtained following general procedure *a* as a pale yellow powder in 90% yield from **2a** and 4-phenoxyphenylboronic acid **27**. RP-HPLC t_R = 24.1 min, gradient condition from 5% B to 100% B in 65 min, flow rate of 4 mL/min, λ = 240 nm. ^1H NMR (300 MHz, MeOD): δ = 7.10−7.20 (m, 4H), 7.25 (t, J = 7.1 Hz, 1H), 7.46 (t, J = 7.5 Hz, 2H), 8.36 (br s, 3H). ESI-MS, calculated for $C_{17}H_{13}N_5O$ 303.1; found m/z = 304.3 $[M + H]^+$.

2-Amino-6-(4-phenoxyphenyl)-9-methylpurine (3e). **3e** was obtained from **3d** following general procedure *b* as a yellow powder in 82% yield. RP-HPLC t_R = 27.5 min, gradient condition from 5% B to 100% B in 75 min, flow rate of 4 mL/min, λ = 240 nm. ^1H NMR (600 MHz, $CDCl_3$): δ = 3.77 (s, 3H), 7.05−7.18 (m, 5H), 7.37 (t, J = 7.8 Hz, 2H), 7.79 (s, 1H), 8.70 (br s, 2H). ^{13}C NMR (150 MHz, $CDCl_3$): δ = 30.6, 118.3, 121.6, 124.8, 125.7, 127.1, 131.2, 133.9, 142.8, 147.6, 150.7, 156.3, 157.8, 163.3. ESI-MS, calculated for $C_{18}H_{15}N_5O$ 317.1; found m/z = 318.2 $[M + H]^+$.

2-Amino-6-(4-(benzyloxy)phenyl)-9*H*-purine (3f). **3f** was obtained following general procedure *a* as a yellow powder in 77% yield from **2a** and 4-(benzyloxy)phenylboronic acid **30**. RP-HPLC t_R = 17.4 min, gradient condition from 5% B to 100% B in 40 min, flow rate of 4 mL/min, λ = 240 nm. ^1H NMR (300 MHz, MeOD): δ = 5.28 (s, 2H), 7.30 (d, J = 8.8 Hz, 2H), 7.36−7.46 (m, 3H), 7.50 (br s, 2H), 8.37−8.45 (m, 3H). ESI-MS, calculated for $C_{18}H_{15}N_5O$ 317.1; found m/z = 318.1 $[M + H]^+$.

2-Amino-6-(4-(3′-(trifluoromethyl)phenoxymethyl)phenyl)-9*H*-purine (3g). **3g** was obtained following general procedure *a* as a yellow powder in 79% yield from **2a** and 4-(3′-(trifluoromethyl)-phenoxymethyl)phenylboronic acid **31**. RP-HPLC t_R = 25.0 min, gradient condition from 5% B to 100% B in 50 min, flow rate of 4 mL/min, λ = 240 nm. ^1H NMR (300 MHz, MeOD): δ = 5.31 (s, 2H), 7.22−7.33 (m, 3H), 7.48 (t, J = 7.9 Hz, 1H), 7.73 (d, J = 8.1 Hz, 2H), 8.37 (br s, 3H). ESI-MS, calculated for $C_{19}H_{14}F_3N_5O$ 385.1; found m/z = 386.1 $[M + H]^+$.

DOI: 10.1021/jm501893k
J. Med. Chem. 2015, 58, 2718−2736

2-Amino-6-(4-((4′-(2-methoxyethyl)phenoxy)methyl)-phenyl)-9*H*-purine (3h). **3h** was obtained following general procedure *a* as a yellow powder in 77% yield from **2a** and 4-((4′-(2-methoxyethyl)phenoxy)methyl)phenylboronic acid **32**. RP-HPLC t_R = 17.9 min, gradient condition from 5% B to 100% B in 40 min, flow rate of 4 mL/min, λ = 240 nm. ^{1}H NMR (300 MHz, MeOD): δ = 2.80 (t, J = 6.9 Hz, 2H), 3.33 (s, 3H), 3.57 (t, J = 6.9 Hz, 2H), 5.22 (s, 2H), 6.96 (d, J = 8.7 Hz, 2H), 7.16 (d, J = 8.6 Hz, 2H), 7.70 (d, J = 8.1 Hz, 2H), 8.33 (s, 1H), 8.40 (d, J = 8.3 Hz, 2H). ESI-MS, calculated for $C_{21}H_{21}N_5O_2$ 375.2; found m/z = 376.1 $[M + H]^+$.

2-Amino-6-(4-benzyloxy-3-chlorophenyl)-9*H*-purine (4a). **4a** was obtained following general procedure *a* as a yellow powder in 84% yield from **2a** and 4-benzyloxy-3-chlorophenylboronic acid **28**. RP-HPLC t_R = 20.4 min, gradient condition from 5% B to 100% B in 40 min, flow rate of 4 mL/min, λ = 240 nm. ^{1}H NMR (300 MHz, MeOD): δ = 5.32 (s, 2H), 7.33−7.44 (m, 4H), 7.50 (br s, 2H), 8.34 (br s, 2H), 8.50 (s, 1H). ESI-MS, calculated for $C_{18}H_{14}ClN_5O$ 351.1; found m/z = 352.1 $[M + H]^+$.

2-Amino-6-(3-chloro-4-(3′,5′-dimethoxybenzyloxy)phenyl)-9*H*-purine (4b). **4b** was obtained following general procedure *a* as a yellow powder in 86% yield from **2a** and 3-chloro-4-(3′,5′-dimethoxybenzyloxy)phenylboronic acid **33**. RP-HPLC t_R = 20.5 min, gradient condition from 5% B to 100% B in 40 min, flow rate of 4 mL/min, λ = 240 nm. ^{1}H NMR (600 MHz, MeOD): δ = 3.76 (s, 6H), 5.28 (s, 2H), 6.48 (s, 1H), 6.68 (s, 2H), 7.32 (d, J = 8.8 Hz, 1H), 8.18 (s, 1H), 8.47 (br s, 1H), 8.61 (s, 1H). ^{13}C NMR (150 MHz, MeOD): δ = 56.2, 71.6, 100.7, 106.2, 115.6, 123.2, 127.0, 128.7, 132.1, 139.7, 143.1, 149.5, 150.3, 155.7, 157.2, 160.4, 161.8. ESI-MS, calculated for $C_{20}H_{18}ClN_5O_3$ 411.1; found m/z = 412.1 $[M + H]^+$.

2-Amino-6-(2,3-dihydrobenzo[*b*][1,4]dioxin-6-yl)-9*H*-purine (4c). **4c** was obtained following general procedure *a* as a pale yellow powder in 84% yield from **2a** and 1,4-benzodioxane-6-boronic acid **26**. RP-HPLC t_R = 11.6. min, gradient condition from 5% B to 100% B in 50 min, flow rate of 4 mL/min, λ = 240 nm. ^{1}H NMR (300 MHz, MeOD): δ = 4.34−4.40 (m, 4H), 7.09 (d, J = 8.5 Hz, 1H), 7.89−7.98 (m, 2H), 8.34 (s, 1H). ESI-MS, calculated for $C_{13}H_{11}N_5O_2$ 269.1; found m/z = 270.2 $[M + H]^+$.

2-Amino-6-(3-(4′-chlorobenzyloxy)phenyl)-9*H*-purine (4d). **4d** was obtained following general procedure *a* as a yellow powder in 78% yield from **2a** and 3-(4′-chlorobenzyloxy)phenylboronic acid **29**. RP-HPLC t_R = 29.8 min, gradient condition from 5% B to 100% B in 70 min, flow rate of 4 mL/min, λ = 240 nm. ^{1}H NMR (300 MHz, MeOD): δ = 5.19 (s, 2H), 7.29 (d, J = 7.6 Hz, 1H), 7.40 (d, J = 8.4 Hz, 2H), 7.45−7.58 (m, 3H), 7.90 (d, J = 6.9 Hz, 1H), 8.01 (s, 1H), 8.37 (s, 1H). ESI-MS, calculated for $C_{18}H_{14}ClN_5O$ 351.1; found m/z = 352.2 $[M + H]^+$.

2-Amino-6-(3-(4′-chlorobenzyloxy)phenyl)-9-methylpurine (4e). **4e** was obtained following general procedure *b* as a yellow powder in 63% yield from **4d**. RP-HPLC t_R = 28.3 min, gradient condition from 5% B to 100% B in 60 min, flow rate of 4 mL/min, λ = 240 nm. ^{1}H NMR (300 MHz, CDCl3): δ = 3.77 (s, 3H), 5.20 (s, 2H), 7.13 (d, J = 7.8 Hz, 1H), 7.36 (d, J = 8.2 Hz, 2H), 7.41−7.51 (m, 3H), 7.83 (s, 1H), 8.31−8.42 (m, 2H). ESI-MS, calculated for $C_{19}H_{16}ClN_5O$ 365.1; found m/z = 366.2 $[M + H]^+$.

2-Amino-6-(3-bromo-5-butoxyphenyl)-9*H*-purine (5a). **5a** was obtained following general procedure *a* as a white powder in 83% yield from **2a** and 3-bromo-5-butoxyphenylboronic acid **21**. RP-HPLC t_R = 26.7 min, gradient condition from 5% B to 100% B in 50 min, flow rate of 4 mL/min, λ = 240 nm. ^{1}H NMR (600 MHz, DMSO-d_6): δ = 0.93 (t, J = 7.3 Hz, 3H), 1.39−1.51 (m, 2H), 1.68−1.76 (m, 2H), 4.06 (t, J = 6.3 Hz, 2H), 6.46 (s, 2H), 7.28 (s, 1H), 8.16 (s, 1H), 8.37 (s, 1H), 8.50 (s, 1H), 12.72 (s, 1H). ^{13}C NMR (150 MHz, DMSO-d_6): δ = 14.9, 20.1, 32.1, 69.5, 115.8, 120.9, 124.4, 125.8, 138.7, 142.2, 148.1, 151.3, 157.2, 161.3. ESI-MS, calculated for $C_{15}H_{16}BrN_5O$ 361.1; found m/z = 362.3 $[M + H]^+$.

2-Amino-6-(3-bromo-5-butoxyphenyl)-9-methylpurine (5b). **5b** was obtained following general procedure *b* as a yellow powder in 85% yield from **5a**. RP-HPLC t_R = 27.9 min, gradient condition from 5% B to 100% B in 45 min, flow rate of 4 mL/min, λ = 240 nm. ^{1}H NMR (300 MHz, CDCl3): δ = 0.97 (t, J = 7.3 Hz, 3H), 1.46−1.55 (m, 2H), 1.73−1.83 (m, 2H), 3.79 (s, 3H), 4.11 (t, J = 6.2 Hz, 2H), 7.29 (s, 1H), 7.92 (s, 1H), 7.97 (s, 1H), 8.33 (s, 1H). ESI-MS, calculated for $C_{16}H_{18}BrN_5O$ 375.1; found m/z = 376.2 $[M + H]^+$.

2-Amino-6-(2,6-dimethoxyphenyl)-9*H*-purine (6a). **6a** was obtained following general procedure *a* as a white powder in 53% yield from **2a** and 2,6-dimethoxyphenylboronic acid **22**. RP-HPLC t_R = 13.0 min, gradient condition from 5% B to 100% B in 80 min, flow rate of 4 mL/min, λ = 240 nm. ^{1}H NMR (300 MHz, MeOD): δ = 3.82 (s, 6H), 6.87 (d, J = 8.5 Hz, 2H), 7.60 (t, J = 8.5 Hz, 1H), 8.44 (s, 1H). ESI-MS, calculated for $C_{13}H_{13}N_5O_2$ 271.1; found m/z = 272.2 $[M + H]^+$.

2-Amino-6-(2-isopropoxy-6-methoxyphenyl)-9*H*-purine (6b). **6b** was obtained following general procedure *a* as a white powder in 62% yield from **2a** and 2-isopropoxy-6-methoxyphenylboronic acid **23**. RP-HPLC t_R = 18.1 min, gradient condition from 5% B to 100% B in 40 min, flow rate of 4 mL/min, λ = 240 nm. ^{1}H NMR (300 MHz, MeOD): δ = 1.18 (s, 6H), 3.80 (s, 3H), 4.60−4.71 (m, 1H), 6.80−6.88 (m, 2H), 7.56 (t, J = 8.5 Hz, 1H), 8.43 (s, 1H). ESI-MS, calculated for $C_{15}H_{17}N_5O_2$ 299.1; found m/z = 300.1 $[M + H]^+$.

2-Amino-6-(2-isobutoxy-6-methoxyphenyl)-9*H*-purine (6c). **6c** was obtained following general procedure *a* as a white powder in 76% yield from **2a** and 2-isobutoxy-6-methoxy-phenylboronic acid **24**. RP-HPLC t_R = 14.2 min, gradient condition from 5% B to 100% B in 40 min, flow rate of 4 mL/min, λ = 240 nm. ^{1}H NMR (600 MHz, DMSO-d_6): δ = 0.69 (s, 6H), 1.72−1.79 (m, 1H), 3.71 (br s, 5H), 6.81−6.86 (m, 2H), 7.52 (t, J = 8.1 Hz, 1H), 8.47 (s, 1H). ^{13}C NMR (150 MHz, MeOD): δ = 20.3, 29.0, 57.6, 76.1, 106.2, 118.6, 125.8, 134.7, 137.4, 142.7, 154.9, 159.3, 160.8, 173.0. ESI-MS, calculated for $C_{16}H_{19}N_5O_2$ 313.2; found m/z = 314.1 $[M + H]^+$.

2-Amino-6-(2-methoxyphenyl)-9*H*-purine (7a). **7a** was obtained following general procedure *a* as a pale yellow powder in 78% yield from **2a** and 2-methoxyphenylboronic acid **15**. RP-HPLC t_R = 14.9 min, gradient condition from 5% B to 100% B in 80 min, flow rate of 4 mL/min, λ = 240 nm. ^{1}H NMR (300 MHz, MeOD): δ = 3.97 (s, 3H), 7.21 (t, J = 7.5 Hz, 1H), 7.30 (d, J = 8.4 Hz, 1H), 7.67 (t, J = 7.8 Hz, 1H), 8.10 (d, J = 7.4 Hz, 1H), 8.45 (s, 1H). ESI-MS, calculated for $C_{12}H_{11}N_5O$ 241.1; found m/z = 242.2 $[M + H]^+$.

2-Amino-6-(5-fluoro-2-methoxyphenyl)-9*H*-purine (7b). **7b** was obtained following general procedure *a* as a pale yellow powder in 70% yield from **2a** and 5-fluoro-2-methoxyphenylboronic acid **16**. RP-HPLC t_R = 14.0 min, gradient condition from 5% B to 100% B in 60 min, flow rate of 4 mL/min, λ = 240 nm. ^{1}H NMR (300 MHz, MeOD): δ = 3.95 (s, 3H), 7.29 (d, J = 8.9 Hz, 1H), 7.41 (dd, J = 8.9, 2.4 Hz, 1H), 7.92 (br s, 1H), 8.54 (s, 1H). ESI-MS, calculated for $C_{12}H_{10}FN_5O$ 259.1; found m/z = 260.1 $[M + H]^+$.

2-Amino-6-(5-chloro-2-methoxyphenyl)-9*H*-purine (7c). **7c** was obtained following general procedure *a* as a pale yellow powder in 78% yield from **2a** and 5-chloro-2-methoxyphenylboronic acid **17**. RP-HPLC t_R = 18.1 min, gradient condition from 5% B to 100% B in 80 min, flow rate of 4 mL/min, λ = 240 nm. ^{1}H NMR (300 MHz, MeOD): δ = 3.95 (s, 3H), 7.28 (d, J = 8.9 Hz, 1H), 7.63 (dd, J = 8.9, 2.5 Hz, 1H), 8.03 (br s, 1H), 8.53 (s, 1H). ESI-MS, calculated for $C_{12}H_{10}ClN_5O$ 275.1; found m/z = 276.1 $[M + H]^+$.

2-Amino-6-(5-bromo-2-methoxyphenyl)-9*H*-purine (7d). **7d** was obtained following general procedure *a* as a yellow powder in 77% yield from **2a** and 5-bromo-2-methoxyphenylboronic acid **18**. RP-HPLC t_R = 17.3 min, gradient condition from 5% B to 100% B in 60 min, flow rate of 4 mL/min, λ = 240 nm. ^{1}H NMR (600 MHz, MeOD): δ = 3.95 (s, 3H), 7.23 (d, J = 9.0 Hz, 1H), 7.76 (dd, J = 8.9, 2.4 Hz, 1H), 8.14 (br s, 1H), 8.53 (s, 1H). ^{13}C NMR (150 MHz, MeOD): δ = 56.3, 113.3, 114.4, 123.7, 126.4, 135.4, 135.9, 142.6, 149.5, 155.1, 157.8, 160.9. ESI-MS, calculated for $C_{12}H_{10}BrN_5O$ 319.0; found m/z = 320.3 $[M + H]^+$.

2-Amino-6-(5-bromo-2-ethoxyphenyl)-9*H*-purine (7e). **7e** was obtained following general procedure *a* as a yellow powder in 82% yield from **2a** and 5-bromo-2-ethoxyphenylboronic acid **19**. RP-HPLC t_R = 21.6 min, gradient condition from 5% B to 100% B in 80 min, flow rate of 4 mL/min, λ = 240 nm. ^{1}H NMR (300 MHz, MeOD): δ = 1.31 (t, J = 6.9 Hz, 3H), 4.13−4.24 (m, 2H), 7.19 (d, J = 8.9 Hz, 1H), 7.72 (dd, J = 8.9, 2.3 Hz, 1H), 7.98 (brs, 1H), 8.53 (s,

DOI: 10.1021/jm501893k
J. Med. Chem. 2015, 58, 2718−2736

1H). ESI-MS, calculated for $C_{13}H_{12}BrN_5O$ 333.0; found m/z = 334.1 $[M + H]^+$.

6-(5-Bromo-2-methoxyphenyl)-2-chloro-9*H*-purine (8a). **8a** was obtained following general procedure *a* as a yellow powder in 68% yield from **1** and 5-bromo-2-methoxyphenylboronic acid **18**. RP-HPLC t_R = 24.3 min, gradient condition from 5% B to 100% B in 45 min, flow rate of 4 mL/min, λ = 240 nm. ^{1}H NMR (300 MHz, CDCl3): δ = 3.91 (s, 3H), 7.00 (d, J = 8.8 Hz, 1H), 7.23 (br s, 1H) 7.63 (d, J = 8.1 Hz, 1H), 8.04 (s, 1H). ESI-MS, calculated for $C_{12}H_8BrClN_4O$ 338.0; found m/z = 339.2 $[M + H]^+$.

2-Amino-6-(5-bromo-2-methoxyphenyl)-9-methylpurine (8b). **8b** was obtained following general procedure *b* as a yellow powder in 87% yield from **7d**. RP-HPLC t_R = 18.9 min, gradient condition from 5% B to 100% B in 70 min, flow rate of 4 mL/min, λ = 240 nm. ^{1}H NMR (300 MHz, CDCl3): δ = 3.79 (s, 3H), 3.87 (s, 3H), 6.94−7.01 (m, 1H), 7.24 (br s, 1H), 8.02 (s, 1H). ESI-MS, calculated for $C_{13}H_{12}BrN_5O$ 333.0; found m/z = 334.2 $[M + H]^+$.

2-Amino-6-(5-bromo-2-methoxyphenyl)-9-(2-oxopropyl)-purine (8c). **8c** was obtained following general procedure *b* as a yellow powder in 50% yield from **7d**. RP-HPLC t_R = 22.9 min, gradient condition from 5% B to 100% B in 80 min, flow rate of 4 mL/min, λ = 240 nm. ^{1}H NMR (600 MHz, $CDCl_3$): δ = 2.40 (s, 3H), 4.01 (s, 3H), 5.00 (s, 2H), 7.03 (d, J = 8.9 Hz, 1H), 7.70 (dd, J = 8.9, 2.4 Hz, 1H), 8.02 (s, 1H), 8.19 (s, 1H). ^{13}C NMR (150 MHz, $CDCl_3$): δ = 27.3, 52.5, 57.1, 114.3, 118.8, 125.1, 126.9, 136.3, 138.4, 143.3, 148.2, 154.3, 156.7, 158.4, 199.2. ESI-MS, calculated for $C_{15}H_{14}BrN_5O_2$ 375.0; found m/z = 376.1 $[M + H]^+$.

6-(5-Fluoro-2-methoxyphenyl)-2-hydroxy-9*H*-purine (8d). **8d** was obtained following general procedure *c* as a white powder in 47% yield from **7b**. RP-HPLC t_R = 13.9 min, gradient condition from 5% B to 100% B in 50 min, flow rate of 1 mL/min, λ = 240 nm. ^{1}H NMR (300 MHz, DMSO-d_6): δ = 3.93 (s, 3H), 7.31 (d, J = 8.9 Hz, 1H), 7.40 (dd, J = 8.9, 2.4 Hz, 1H), 7.89 (br s, 1H), 8.54 (s, 1H). ESI-MS, calculated for $C_{12}H_9FN_4O_2$ 260.1; found m/z = 261.1 $[M + H]^+$.

6-(5-Chloro-2-methoxyphenyl)-2-hydroxy-9*H*-purine (8e). **8e** was obtained following general procedure *c* as a white powder in 63% yield from **7c**. RP-HPLC t_R = 14.8 min, gradient condition from 5% B to 100% B in 50 min, flow rate of 4 mL/min, λ = 240 nm. ^{1}H NMR (300 MHz, DMSO-d_6): δ = 3.94 (s, 3H), 7.26 (d, J = 8.9 Hz, 1H), 7.63 (dd, J = 8.9, 2.5 Hz, 1H), 8.03 (br s, 1H), 8.53 (s, 1H). ESI-MS, calculated for $C_{12}H_9ClN_4O_2$ 276.0; found m/z = 277.1 $[M + H]^+$.

6-(5-Bromo-2-methoxyphenyl)-2-hydroxy-9*H*-purine (8f). **8f** was obtained following general procedure *c* as a white powder in 55% yield from **7d**. RP-HPLC t_R = 15.8 min, gradient condition from 5% B to 100% B in 50 min, flow rate of 1 mL/min, λ = 240 nm. ^{1}H NMR (300 MHz, DMSO-d_6): δ = 3.97 (s, 3H), 7.25 (d, J = 9.0 Hz, 1H), 7.76 (dd, J = 8.9, 2.4 Hz, 1H), 8.14 (br s, 1H), 8.53 (s, 1H). ESI-MS, calculated for $C_{12}H_9BrN_4O_2$ 320.0; found m/z = 321.1$[M + H]^+$.

6-(5-Bromo-2-methoxyphenyl)-8-methyl-9*H*-purine (9a). **9a** was obtained following general procedure *a* as a pale yellow powder in 70% yield from 6-chloro-8-methyl-9*H*-purine **12** and 5-bromo-2-methoxyphenylboronic acid **18**. RP-HPLC t_R = 21.7 min, gradient condition from 5% B to 100% B in 70 min, flow rate of 4 mL/min, λ = 240 nm. ^{1}H NMR (300 MHz, DMSO-d_6): δ = 2.69 (s, 3H), 3.87 (s, 3H), 7.20 (d, J = 9.0 Hz, 1H), 7.71 (dd, J = 8.9, 2.4 Hz, 1H), 7.82 (s, 1H), 8.95 (s, 1H). ESI-MS, calculated for $C_{13}H_{11}BrN_4O$ 318.0; found m/z = 319.2 $[M + H]^+$.

6-(5-Fluoro-2-methoxyphenyl)-8-methyl-9*H*-purine (9b). **9b** was obtained following general procedure *a* as a pale yellow powder in 81% yield from 6-chloro-8-methyl-9*H*-purine **12** and 5-fluoro-2-methoxyphenylboronic acid **16**. RP-HPLC t_R = 15.6 min, gradient condition from 5% B to 100% B in 60 min, flow rate of 4 mL/min, λ = 240 nm. ^{1}H NMR (300 MHz, MeOD): δ = 2.76 (s, 3H), 3.90 (s, 3H), 7.27 (d, J = 9.0 Hz, 1H), 7.39 (br s, 1H), 7.67 (dd, J = 8.9, 2.4 Hz, 1H), 9.04 (s, 1H). ^{13}C NMR (75 MHz, MeOD): δ = 14.1, 56.2, 113.5, 117.9, 118.3, 119.2, 126.9, 147.7, 151.3, 154.5, 155.9, 158.2, 159.2. ESI-MS, calculated for $C_{13}H_{11}FN_4O$ 258.1; found m/z = 259.1 $[M + H]^+$.

2-Amino-6-thianthrenyl-9*H*-purine (10). **10** was obtained following general procedure *a* as a yellow powder in 82% yield from **2a** and 1-thianthrenylboronic acid **25**. RP-HPLC t_R = 18.5 min, gradient condition from 5% B to 100% B in 40 min, flow rate of 4 mL/min, λ = 240 nm. ^{1}H NMR (300 MHz, MeOD): δ = 7.22−7.37 (m, 3H), 7.51 (t, J = 7.5 Hz, 2H), 7.65 (d, J = 7.4 Hz, 1H), 7.75 (d, J = 7.7 Hz, 1H), 8.37 (s, 1H). ESI-MS, calculated for $C_{17}H_{11}N_5S_2$ 349.0; found m/z = 350.1 $[M + H]^+$.

2-Amino-6-(5-bromo-2,3-dihydrobenzo[*b*]furan-7-yl)-9*H*-purine (11). **11** was obtained following general procedure *a* as a pale yellow powder in 79% yield from **2a** and 5-bromo-2,3-dihydrobenzo-[*b*]furan-7-boronic acid **20**. RP-HPLC t_R = 15.2 min, gradient condition from 5% B to 100% B in 40 min, flow rate of 4 mL/min, λ = 240 nm. ^{1}H NMR (600 MHz, MeOD): δ = 3.35−3.42 (m, 2H), 4.87−4.93 (m, 2H), 7.65 (s, 1H), 8.50 (s, 1H), 8.57 (s, 1H). ^{13}C NMR (150 MHz, MeOD): δ = 29.1, 74.3, 113.6, 121.2, 125.8, 131.5, 132.1, 134.0, 146.1, 154.9, 158.8, 159.9, 160.7. ESI-MS, calculated for $C_{13}H_{10}BrN_5O$ 331.0; found m/z = 332.2 $[M + H]^+$.

Protein Expression and Purification. Proteins were cloned, expressed, and purified as previously described.[23]

Protein Stability Shift Assay. Thermal melting experiments were carried out using an Mx3005p real time PCR machine (Stratagene). Proteins were buffered in 10 mM HEPES, pH 7.5, 500 mM NaCl and assayed in a 96-well plate at a final concentration of 2 μM in 20 μL volume. Compounds were added at a final concentration of 10 or 100 μM. SYPRO Orange (Molecular Probes) was added as a fluorescence probe at a dilution of 1 in 1000. Excitation and emission filters for the SYPRO-Orange dye were set to 465 and 590 nm, respectively. The temperature was raised with a step of 3 °C per minute from 25 to 96 °C, and fluorescence readings were taken at each interval. The temperature dependence of the fluorescence during the protein denaturation process was approximated by the equation

$$y(T) = y_F + \frac{y_U - y_F}{1 + e^{\Delta uG_{(T)}/(RT)}}$$

where ΔuG is the difference in unfolding free energy between the folded and unfolded state, R is the gas constant, and y_F and y_U are the fluorescence intensity of the probe in the presence of completely folded and unfolded protein, respectively.[65] The baselines of the denatured and native states were approximated by a linear fit. The observed temperature shifts, ΔT_m^{obs}, were recorded as the difference between the transition midpoints of sample and reference wells containing protein without ligand in the same plate and determined by nonlinear least-squares fit. Temperature shifts (ΔT_m^{obs}) for three independent measurements per proteins/compound are summarized in Supporting Information Table S1.

Isothermal Titration Calorimetry. Experiments were carried out on an ITC200 titration microcalorimeter from MicroCal, LLC (GE Healthcare) equipped with a Washing module, with a cell volume of 0.2003 mL, and a 40 μL microsyringe. Experiments were carried out at 15 °C while stirring at 1000 rpm, in ITC buffer (50 mM HEPES, pH 7.5 (at 25 °C), 150 mM NaCl). The microsyringe was loaded with a solution of the protein sample (300−740 μM protein for BRD9 and BRD4(1), respectively, in ITC buffer) and was carefully inserted into the calorimetric cell which was filled with an amount of the ligand (0.2 mL, 20−25 μM in ITC buffer). The system was first allowed to equilibrate until the cell temperature reached 15 °C, and an additional delay of 60 s was applied. All titrations were conducted using an initial control injection of 0.3 μL followed by 38 identical injections of 1 μL with a duration of 2 s (per injection) and a spacing of 120 s between injections. The titration experiments were designed in such a fashion as to ensure complete saturation of the proteins before the final injection. The heat of dilution for the proteins was independent of their concentration and corresponded to the heat observed from the last injection, following saturation of ligand binding, thus facilitating the estimation of the baseline of each titration from the last injection. The collected data were corrected for protein heats of dilution (measured on separate experiments by titrating the proteins into ITC buffer) and deconvoluted using the MicroCal Origin software supplied with the instrument to yield enthalpies of binding (ΔH) and binding constants (K_B) in the same fashion as that previously described in detail by Wiseman and co-workers.[66] Thermodynamic parameters were calculated using the basic equation of thermodynamics (ΔG =

DOI: 10.1021/jm501893k
J. Med. Chem. 2015, 58, 2718−2736

Table 1. Isothermal Titration Calorimetry of Human BRD4(1) with 9*H*-Purine Compounds[a]

ligand	[P] (μM)	[L] (μM)	K_D (nM)	ΔH^{obs} (kcal/mol)	N	$T\Delta S$ (kcal/mol)	ΔG (kcal/mol)	LE
2a	680	15			no binding/weak			
3a	402	16	11990 ± 743	−9.45 ± 0.55	1.03 ± 0.049	−2.97	−6.48	0.41
7c	485	14	2037 ± 118	−6.21 ± 0.09	1.05 ± 0.012	1.29	−7.50	0.39
7d	307	12	4651 ± 197	−6.09 ± 0.14	0.99 ± 0.018	0.94	−7.03	0.37
11	382	30	1370 ± 29	−6.39 ± 0.02	1.09 ± 0.002	1.34	−7.73	0.39

[a]Titrations were carried out in 50 mM HEPES, pH 7.5 (at 25 °C), 150 mM NaCl, and 15 °C while stirring at 1000 rpm. In both cases the protein was titrated into the ligand solution (reverse titration). Titrations were performed in triplicate. Ligand efficiencies (LE) have also been calculated where ΔG values were available (LE = $\Delta G/N$ where N is the number of non-hydrogen atoms).

Table 2. Isothermal Titration Calorimetry of Human BRD9 with 9*H*-Purine Compounds[a]

ligand	[P] (μM)	[L] (μM)	K_D (nM)	ΔH^{obs} (kcal/mol)	N	$T\Delta S$ (kcal/mol)	ΔG (kcal/mol)	LE
2a	740	30			no binding/weak			
2b	385	30			no binding/weak			
3a	477	26	8475 ± 237	−9.11 ± 0.12	0.99 ± 0.010	−2.42	−6.69	0.42
5b	392	30			no binding/weak			
7a	385	34	641 ± 33	−12.71 ± 0.07	1.06 ± 0.004	−4.55	−8.16	0.45
7b	385	13.5	351 ± 18	−13.04 ± 0.07	0.97 ± 0.004	−4.52	−8.52	0.45
7c	378	14	297 ± 10	−12.05 ± 0.04	0.98 ± 0.003	−3.46	−8.59	0.45
7d	235	10	397 ± 19	−9.63 ± 0.06	0.97 ± 0.005	−1.18	−8.45	0.44
8a	381	18	7874 ± 258	−8.30 ± 0.15	1.06 ± 0.014	−1.57	−6.73	0.35
8b	392	30			no binding/weak			
8e	451	32	7576 ± 365	−5.35 ± 0.09	1.05 ± 0.013	1.40	−6.75	0.36
9a	378	20			no binding/weak			
11	381	30	278 ± 15	−10.28 ± 0.04	1.03 ± 0.003	−1.63	−8.65	0.43

[a]Titrations were carried out in 50 mM HEPES, pH 7.5 (at 25 °C), 150 mM NaCl, and 15 °C while stirring at 1000 rpm. In both cases the protein was titrated into the ligand solution (reverse titration). Titrations were performed in triplicate. Ligand efficiencies (LE) have also been calculated where ΔG values were available (LE = $\Delta G/N$ where N is the number of non-hydrogen atoms).

$\Delta H - T\Delta S = -RT \ln K_B$, where ΔG, ΔH, and ΔS are the changes in free energy, enthalpy, and entropy of binding, respectively). In all cases a single binding site model was employed, supplied with the MicroCal Origin software package. Dissociation constants and thermodynamic parameters are listed in Tables 1, 2, and 3.

Bioluminescence Resonance Energy Transfer Assay (BRET). HEK293 cells (8×10^5) were plated in each well of a 6-well plate and co-transfected with histone H3.3-HaloTag (NM_002107) and NanoLuc-BRD9 (Q9H8M2-BRD amino acids 120−240) or NanoLuc-BRD4 full-length (060885). Twenty hours post-transfection 2×10^4 cells were trypsinized, washed with PBS, and exchanged into media containing phenol red-free DMEM, 10% FBS in the absence (control sample), or the presence (experimental sample) of 100 nM NanoBRET 618 fluorescent ligand (Promega). Cell density was adjusted to 2×10^5 cells/mL and then replated in a 96-well assay white plate (Corning Costar no. 3917). At the time of replating compound **7d** or **11** were added at a final concentration spanning from 0.005 to 33 μM and the plates were incubated for 18 h at 37 °C in the presence of 5% CO_2. NanoBRET substrate (Promega) was added to both control and experimental samples at a final concentration of 10 μM. Readings were performed within 5 min using the CLARIOstar reader (BMG Lifetechnologies) equipped with 450/80 nm bandpass and 610 nm long-pass filters. A corrected BRET ratio was calculated and is defined as the ratio of the emission at 610 nm/450 nm for experimental samples (i.e., those treated with NanoBRET fluorescent ligand) subtracted by and the emission at 610 nm/450 nm for control samples (not treated with NanoBRET fluorescent). BRET ratios are expressed as milliBRET units (mBU), where 1 mBU corresponds to the corrected BRET ratio multiplied by 1000.

Confocal Imaging. HEK293 cells were transfected with histone H3.3-HaloTag using FuGENE HD (Promega). Twenty-four hours post-transfection cells were labeled with 5 μM HaloTag TMR ligand (Promega) in complete medium (DMEM and 10% FBS) for 15 min at 37 °C and 5% CO_2. Medium containing HaloTag-TMR ligand was then washed twice with fresh complete medium. Cells were placed back at 37 °C and 5% CO_2 for 30 min and then imaged. Images were acquired on an Olympus Fluoview FV500 confocal microscope (Olympus, Center Valley, PA, USA) containing a 37 °C and CO_2 environmental chamber (Solent Scientific Ltd., Segensworth, U.K.) using appropriate filter sets.

In Vitro Cytotoxicity. Following NanoBRET substrate addition and NanoBRET measurements, to the same wells an equal volume of CellTiter-Glo reagent (Promega) was added and the plates were incubated for 30 min at room temperature. Total luminescence was measured, and relative compound toxicity was determined by comparing the RLUs (relative light units) of a sample containing DMSO vehicle (in the absence of compound **11**) to the RLUs of the samples containing 0.005−33 μM compound **11**.

Crystallization. Aliquots of the purified proteins were set up for crystallization using a mosquito crystallization robot (TTP Labtech, Royston, U.K.). Coarse screens were typically set up onto Greiner 3-well plates using three different drop ratios of precipitant to protein per condition (100 + 50 nL, 75 + 75 nL, and 50 + 100 nL). Initial hits were optimized further scaling up the drop sizes. All crystallizations were carried out using the sitting drop vapor diffusion method at 4 °C. BRD9 crystals with **7d** were grown by mixing 150 nL of the protein (17.9 mg/mL and 2 mM final ligand concentration) with 150 nL of reservoir solution containing 0.20 M sodium bromate, 0.1 M BT-propane, pH 7.5, 20% PEG3350, and 10% ethylene glycol. BRD4(1) crystals with **7d** were grown by mixing 200 nL of protein (12 mg/mL and 2 mM final ligand concentration) with 100 nL of reservoir solution containing 0.2 M sodium nitrate, 20% PEG3350, and 10% ethylene glycol. BRD4(1) crystals with **11** were grown by mixing 150 nL of protein (8.25 mg/mL and 2 mM final ligand concentration) with 150 nL of reservoir solution containing 0.1 M bis-tris-propane, pH 8.5, 20% PEG3350, and 10% ethylene glycol. In all cases diffraction quality crystals grew within a few days.

Data Collection and Structure Solution. All crystals were cryoprotected using the well solution supplemented with additional ethylene glycol and were flash frozen in liquid nitrogen. Data were

DOI: 10.1021/jm501893k
J. Med. Chem. 2015, 58, 2718−2736

Table 3. Isothermal Titration Calorimetry of Human BRD2 and BRD3 with Selected 9*H*-Purine Compounds[a]

protein/ligand	[P] (μM)	[L] (μM)	K_D (nM)	ΔH^{obs} (kcal/mol)	N	$T\Delta S$ (kcal/mol)	ΔG (kcal/mol)	LE
BRD2(1)/**7d**	518	20	4444 ± 162	−6.62 ± 0.09	0.99 ± 0.011	0.44	−7.06	0.37
BRD3(1)/**7d**	532	20	2037 ± 105	−7.17 ± 0.09	1.01 ± 0.009	0.33	−7.50	0.39
BRD2(1)/**11**	488	20	1421 ± 60	−5.65 ± 0.04	1.02 ± 0.006	2.06	−7.71	0.39
BRD3(1)/**11**	510	20	2037 ± 105	−7.17 ± 0.09	1.01 ± 0.009	0.33	−7.50	0.38

[a]Titrations were carried out in 50 mM HEPES, pH 7.5 (at 25 °C), 150 mM NaCl, and 15 °C while stirring at 1000 rpm. In both cases the protein was titrated into the ligand solution (reverse titration). Titrations were performed in triplicate. Ligand efficiencies (LE) have also been calculated where ΔG values were available (LE = $\Delta G/N$ where N is the number of non-hydrogen atoms).

Table 4. Data Collection and Refinement Statistics for Compound 7d Complexes with BRD9 and BRD4(1) and Compound 11 with BRD4(1)

	Data Collection		
	PDB code		
	4XY8	4XY9	4XYA
protein/ligand	BRD9/**7d**	BRD4(1)/**7d**	BRD4(1)/**11**
space group	C2	$P2_12_12_1$	$P2_12_12_1$
cell dimensions			
a, *b*, *c* (Å)	80.63, 43.58, 40.81	37.23, 44.12, 78.58	37.24, 44.37, 79.01
α, β, γ (deg)	90.00, 104.25, 90.00	90.00, 90.00, 90.00	90.00, 90.00, 90.00
resolution[a] (Å)	1.70 (1.79−1.70)	1.68 (1.77−1.68)	2.05 (2.15−2.05)
unique observations[a]	14841 (2064)	15354 (2213)	8708 (1126)
completeness[a] (%)	97.7 (95.2)	99.8 (99.4)	99.9 (99.9)
redundancy[a]	9.6 (9.4)	5.3 (5.0)	4.7 (3.2)
R_{merge}[a]	0.086 (0.337)	0.154 (0.802)	0.079 (0.205)
$I/\sigma I$[a]	20.3 (7.4)	8.2 (2.0)	12.4 (4.9)
	Refinement		
resolution (Å)	1.60	1.68	2.05
R_{work}/R_{free} (%)	17.4/27.5	25.9/28.1	14.9/20.7
no. of atoms (protein/other/water)	933/20/191	1059/27/143	1056/24/148
B-factors (Å^2) (protein/other/water)	14.23/6.78/27.23	14.21/22.85/24.34	13.99/10.49/22.04
rmsd bonds (Å)	0.016	0.016	0.015
rmsd angles (deg)	1.747	1.680	1.652
Ramachadran			
favored (%)	98.17	97.60	97.60
allowed (%)	1.83	2.40	2.40
disallowed (%)	0.00	0.00	0.00

[a]Values in parentheses correspond to the highest resolution shell.

collected in-house on a Rigaku FRE rotating anode system equipped with a RAXIS-IV detector at 1.52 Å (BRD9/**7d**) or on a Bruker MicroStar equipped with an APEX II detector at 1.54 Å (BRD4(1)/**7d** and BRD4(1)/**11**). Indexing and integration were carried out using SAINT (version 8.3, Bruker AXS Inc., 2013) or MOSFLM[67] or XDS,[68,69] and scaling was performed with SCALA[70] or XPREP (version 2008/2, Bruker AXS Inc.). Initial phases were calculated by molecular replacement with PHASER[71] using the known models of BRD9 and BRD4(1) (PDB codes 3HME and 2OSS, respectively). Initial models were built by ARP/wARP[72] followed by manual building in COOT.[73] Refinement was carried out in REFMAC5.[74] In all cases thermal motions were analyzed using TLSMD[75] and hydrogen atoms were included in late refinement cycles. Data collection and refinement statistics can be found in Table 4. The models and structure factors have been deposited in the PDB with accession codes 4XY8 (BRD9/**7d**), 4XY9 (BRD4(1)/**7d**), and 4XYA (BRD4(1)/**11**).

RESULTS AND DISCUSSION

In order to assess the binding of purine fragments on human BRDs, we first performed molecular docking experiments employing the previously determined crystal structure of the complex of BRD4(1) with a 5-methyltriazolopyrimidine ligand (PDB code 4MEN[30]). To this end we investigated binding of purine fragments **1**, **2a**, and **2b** (Figure 1B), seeking to determine acetyllysine competitive binding modes within the BRD cavity with promising predicted binding affinities, ideally establishing favorable interactions with residues implicated in acetyllysine peptide recognition. In order to account for putative conformational changes of the receptor's binding site cavity upon ligand binding, we employed the Induced Fit docking protocol[61,62] (as implemented in the Schrödinger software package). Molecular modeling resulted in good accommodation of the investigated purine fragments within the Kac binding site of BRD4(1), mainly packing between the ZA-loop hydrophobic residues (Val87, Leu92, Leu94) and Ile146 from helix C, in a groove that is capped on one end by Tyr97 and Tyr139 and Trp81 on the other end (Figure 1C). We observed different conformations of compound **1** within the BRD4(1) cavity, with the two chloro functions pointing to the top of the pocket (Figure 1C) or adopting a Kac mimetic pose with one chlorine inserting deep into the pocket (Figure 1D). Compound **2a** was also found in two different states in our calculations, either orienting its primary amine function away from the conserved asparagine (Asn140, Figure 1E) or

DOI: 10.1021/jm501893k
J. Med. Chem. 2015, 58, 2718−2736

Scheme 1. General Procedures for the Synthesis of Purine Derivatives: (A) Suzuki–Miyaura Cross-Coupling of Free Halopurines and (B) TBAF-Assisted N-9 Alkylation on the Purine Ring[a]

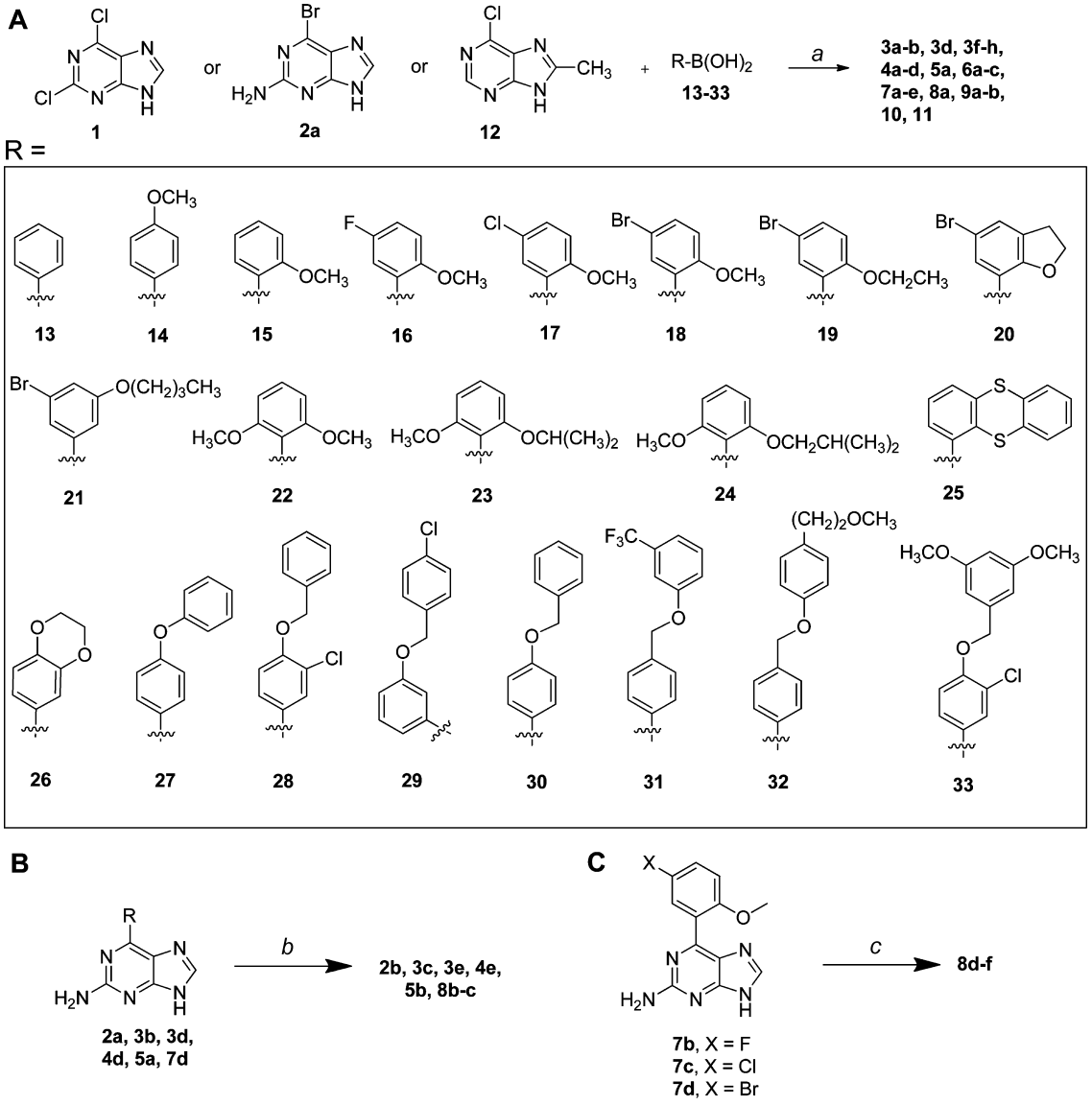

[a]Reagents and conditions: (a) $Pd(OAc)_2/P(C_6H_4SO_3Na)_3$, Cs_2CO_3, $MeCN/H_2O$ (1:2), microwaves, 150 °C, 5–15 min; (b) CH_3I or CH_3COCH_2Cl, TBAF, THF, rt, 10 min; (c) 50% H_2SO_4, $NaNO_2$, −10 °C, 2 h, then 50 °C, 1 h.

directly engaging this residue while orienting its 6-Br substituent toward the ZA-loop (Supporting Information Figure 1A,B). In all cases the ligand poses resulted in promising predicted binding energy values (−9.13 kcal/mol for **1**, −9.95 kcal/mol for **2a**, and −9.13 kcal/mol for **2b**). We identified in our calculations, in the case of compound **2a**, poses that exposed the halogen in position 6 so that the purine core scaffold may be further optimized based on its topology within the BRD binding site. The opposite was true in the case of the 2-Cl substituent or the methyl substituent at N9 (**1** or **2b**, respectively), which resulted in steric clashes and topologies that would not allow for subsequent optimizations. To better understand the binding mode of the purine scaffold to BRDs, given the multiple docking conformations observed, we decided to systematically probe the topology of these fragments employing synthetic chemistry and structure–activity relationships.

We purchased 2,6-dichloro-9*H*-purine **1** and 2-amino-6-bromo-9*H*-purine **2a** and synthesized compound **2b** employing a TBAF-assisted N-9 methylation on the purine ring of **2a**. To confirm binding of these fragments to human bromodomains, we employed a thermal shift assay (ΔT_m assay) which we have previously used successfully with fragments and various human bromodomains.[23,26,28,76,77] Typically we perform the assay using 100 μM compounds in the case of fragments and very weak ligands, but in the case of the purine analogues tested we were surprised to see binding at 10 μM compound to BET BRDs and in particular to BRD4(1); however, the optimized CDK inhibitor olomoucine did not show any significant stabilization toward any proteins in the panel (Figure 1F, Supporting Information Table S1). Encouraged by this result, we tested these compounds at the same concentration against five other diverse BRDs in an effort to cover most of the human BRD phylogenetic tree (Supporting Information Figure 1C) and found that despite their structural diversity, the BRDs of

DOI: 10.1021/jm501893k
J. Med. Chem. 2015, 58, 2718–2736

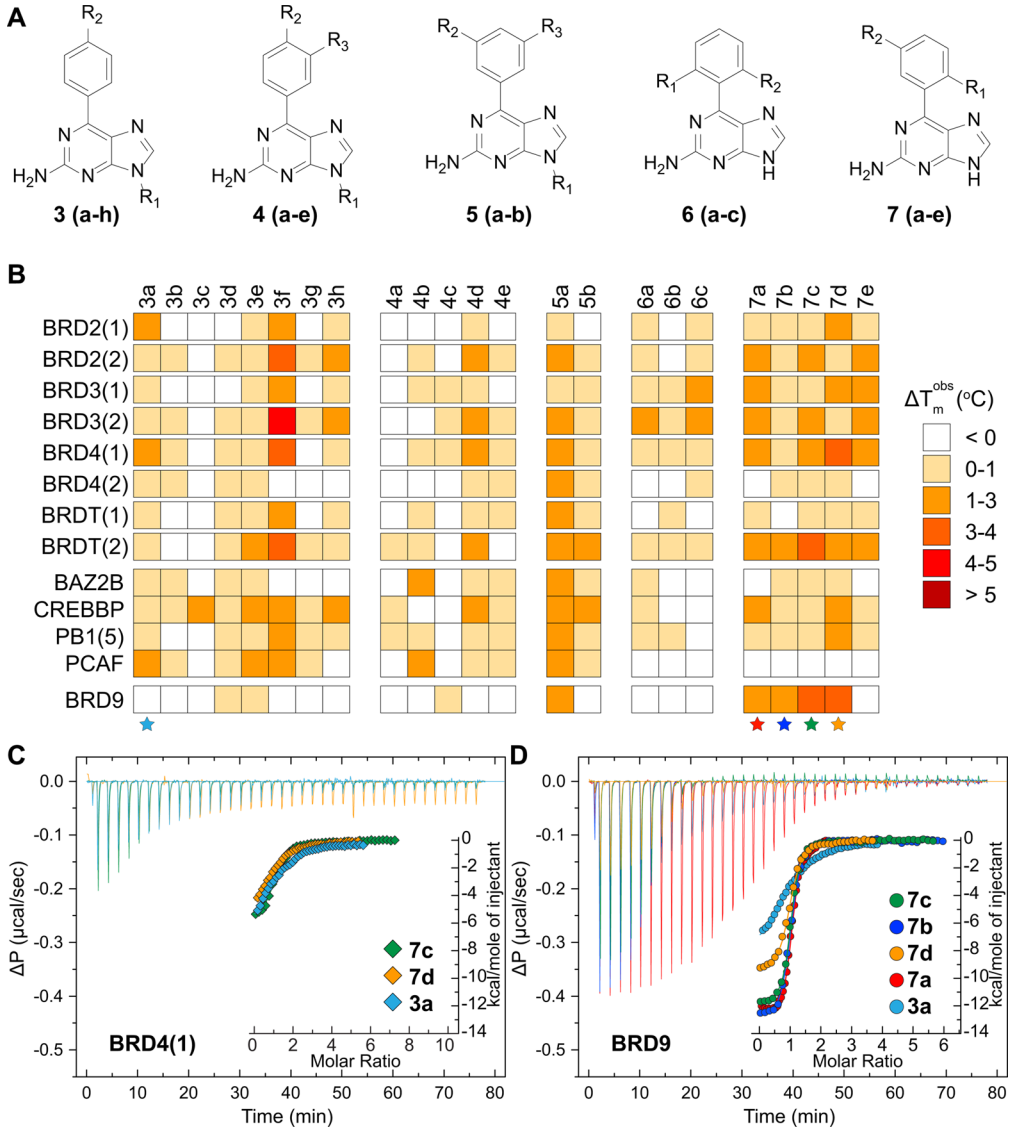

Figure 2. SAR of 9*H*-purines. The 9*H*-purine core scaffold was iteratively decorated and tested for binding to human bromodomains. (A) Substitution patterns explored. (B) Thermal shift assay against human bromodomains. Thermal shifts are color-coded as indicated in the inset. Compounds highlighted with a colored star were further validated by isothermal titration calorimetry as shown in (C)/(D). (C) Isothermal titration calorimetry validation of key compounds binding to BRD4(1) showing raw injection heats for titrations of protein into compound. The inset shows the normalized binding enthalpies corrected for the heat of protein dilution as a function of binding site saturation (symbols as indicated in the figure). Solid lines represent a nonlinear least-squares fit using a single-site binding model. (D) Compounds bearing ortho,meta′ substitutions gain potency toward BRD9 as demonstrated by ITC experiments. Data have been corrected and displayed as described in (C). All ITC titrations were carried out in 50 mM HEPES, pH 7.5 (at 25 °C), 150 mM NaCl, and 15 °C while stirring at 1000 rpm.

CREBBP, PB1(5), and BRD9 exhibited weak binding. We were particularly intrigued by the interaction of **2a** with BRD9, since to our knowledge only a small subset of compounds has been previously shown to bind to this module.[33] To further evaluate binding of **2a** onto BRD9, we performed docking experiments, using the recently crystallized apo structure of the protein (PDB code 3HME[15]) accounting for the flexibility of key residues after ligand binding.[61,62] Similar to our BRD4(1) docking experiment, we obtained two main binding poses for this compound, with the most energetically favored one (predicted binding affinity of −9.06 kcal/mol) exhibiting an extended hydrogen bond network with the conserved Asn100 and $\pi-\pi$ interactions with the ZA-loop Tyr57 and Tyr106 from helix C, while the 6-Br substituent was found oriented toward the external part of the binding site toward the ZA-loop Phe47, suggesting that modifications on this position for subsequent optimization would not be tolerated without affecting the ligand orientation in the acetyllysine cavity (Supporting Information Figure 1D). Conversely, we observed subtle rearrangement of the side chains of Phe44 and Tyr106 accompanied by almost a 90° rotation of the side chain of Phe47, suggesting an induced-fit binding mode. We also observed an alternative binding pose (predicted binding energy of −8.62 kcal/mol) in which the ligand maintained the hydrogen bond to Asn100, albeit from its primary amine function which inserted toward the conserved asparagine, as well as the $\pi-\pi$ interaction with Tyr106 from helix C, while orienting the modifiable 6-Br substituent toward the top of the BRD cavity (Supporting Information Figure 1E), offering a promising vector for subsequent modifications. Using both

DOI: 10.1021/jm501893k
J. Med. Chem. 2015, 58, 2718−2736

possible orientations as starting points, we decided to further interrogate how the purine core scaffold binds to this BRD.

Encouraged by our initial findings, we synthesized a number of 2-amino-9*H*-purine analogues and tested their ability to interact with human BRDs, primarily of the BET subfamily (subfamily II), while systematically testing binding to representative BRDs from other structural subfamilies (family I, PCAF; family III, CREBBP; family IV, BRD9; family V, BAZ2B; family VIII, PB1(5); see Supporting Information Figure 1C) in order to probe structurally diverse proteins against this core purine scaffold. We utilized an aqueous-phase Suzuki−Miyaura cross-coupling reaction to synthesize 2-amino-6-aryl-9*H*-purine derivatives, yielding highly C-6 decorated 9*H*-purines in a one-step procedure and performed a subsequent TBAF-assisted N-9 alkylation to access N-9 substituted analogues (Scheme 1 and Chart 2). We accomplished the coupling step under microwave irradiation with $Pd(OAc)_2$ and triphenylphosphine-3,3′,3″-trisulfonic acid trisodium salt as the catalytic system, with Cs_2CO_3 as base, in a water−acetonitrile reaction solvent. This approach allowed synthesizing 2-amino-6-aryl-9*H*-purines with very short reaction times (5−15 min) at high yields and purity.

First we introduced a phenyl substituent at position 6 of the core purine scaffold (compound **3a**) only to find that BRD2(1), BRD4(1), and PCAF were stabilized in thermal melt assays by this compound (Figure 2A,B). We confirmed binding to BRD4(1) by isothermal titration calorimetry and measured a dissociation constant of 11.99 μM (Figure 2C and Table 1). The interaction of **3a** with BRD4(1) was mainly driven by enthalpic contributions (ΔH = −9.45 kcal/mol), opposed by negative entropy ($T\Delta S$ = −2.97 kcal/mol). We were also intrigued by the lack of affinity toward BRD9 in the ΔT_m assay, since our initial fragment hit, compound **2a**, had exhibited a thermal shift of 1.6 °C toward that domain. We therefore tested this scaffold by isothermal titration calorimetry against BRD9 and measured a weak dissociation constant of 8.5 μM (Figure 2D, Table 2) suggesting that our primary assay (ΔT_m) may not be very robust in the case of BRD9 when applied to weak ligands. This is important, since the first bromodomain of BRD4 has been repeatedly shown to bind to weak compounds employing this assay,[76] while it has been noted that other BRDs do not always exhibit high temperature shifts although they bind to several compounds very potently.[37] Additionally, in the case of BET proteins it has been demonstrated that thermal melt data correlate well with in vitro dissociation constants.[23] Importantly, similar to the BRD4(1)/**3a** interaction, the compound interacted with BRD9 mainly driven by enthalpic contributions (ΔH = −9.11 kcal/mol) opposed by negative entropy ($T\Delta S$ = −2.42 kcal/mol).

In order to better explore the structure−activity relationship of 6-phenyl substituted 9*H*-purines, we synthesized a range of compounds carrying different patterns of functions, including para-substitutions (compounds **3b**−**h**), meta,para substitutions (compounds **4a**−**e**), meta,meta′ substitutions (compounds **5a**,**b**), ortho,ortho′ substitutions (compounds **6a**−**c**), and ortho,meta′ substitutions (compounds **7a**−**e**) (Figure 2A and Chart 2). We tested binding of these analogues to the eight BET BRDs, as well as the five more diverse BRDs previously mentioned, employing the same thermal shift assay as above. Interestingly, compounds synthesized that carried an additional methyl modification at N9 (compounds **3c**, **3e**, **4e**, **5b**) exhibited very weak or no binding toward most BRDs while showing small thermal shits (1.0−1.3 °C) for the bromodomain of CREBBP. Para substitution of the 6-phenyl-9*H*-purines (compounds **3b**−**h**) resulted in lower stabilization of all BRDs; however, compound **3f** showed binding toward all BRDs without any hints of selectivity toward BRD9. Meta substitutions (compounds **4a**−**e**) were also very weak across BRDs with no affinity for BRD9, suggesting that modifications on that vector were not tolerated. Interestingly meta,meta′ substitution (compound **5a**) resulted in binding to most BRDs albeit weak, with ΔT_m values between 1.1 and 1.8 °C. As expected, this binding event was abolished when the compound was methylated at N9 (compound **5b**). Binding was not improved with ortho,ortho′ substitutions of the 6-phenyl 9*H*-purine scaffold (compounds **6a**−**c**) (Figure 2B and Supporting Information Table S1). Since methyl substitution at N9 could not be tolerated in BRD4(1) or BRD9 binding, we concluded at this stage that the five-membered ring is probably not oriented toward the top of the BRD cavity but points toward the bottom of the acetyllysine binding cavity, as predicted in our docking model (Supporting Information Figure 1A,B), with the 6-substituted position toward the front of the pocket in order to accommodate the larger phenyl-substituted functions.

We decided to further test combinations in ortho,meta′ substituted compounds by first maintaining a methoxy functionality at the ortho position while changing the steric bulk at the meta′ position (compounds **7a**−**d**). 2-Methoxyphenyl substitution (compound **7a**) yielded thermal shifts between 1.4 and 2.5 °C for BET BRDs as well as 1.5 °C for the BRD of CREBBP while significantly stabilizing BRD9 compared to all previous compounds tested (2.9 °C). We confirmed this binding by ITC and measured a dissociation constant of 641 nM against BRD9 (Figure 2D, Table 2). Notably the change in affinity was accompanied by negative entropic contributions ($T\Delta S$ = −4.55 kcal/mol). Intrigued by this step change in affinity, we tested halide analogues at the meta′ position while retaining the ortho-methoxy functionality (compounds **7b**−**d**) and observed improved thermal shifts for all compounds tested against BRD9, while BET affinity seemed to be variable. Notably, we observed ΔT_m values following the order H < F < Cl > Br, suggesting that steric bulk and charge at the meta′ position is important, with compound **7c** showing a ΔT_m of 3.8 °C against BRD9. We validated binding using ITC as an orthogonal method and measured dissociation constants of 351, 297, and 397 nM against BRD9 following the same ranking as the thermal shift assay for compounds **7b**, **7c**, and **7d**, respectively (Figure 2D, Table 2). Importantly, we observed a gradual increase in entropic contributions with increasing bulk of the 5-halide-2-methoxyphenyl substitution, with compound **7a** exhibiting the lowest entropic term ($T\Delta S$ = −4.55 kcal/mol) and compound **7d** the highest ($T\Delta S$ = −1.57 kcal/mol). Interestingly, BRD4(1), which exhibited ΔT_m values of 1.1 and 3.2 °C for compounds **7c** and **7d**, was found to bind weakly to these scaffolds by ITC, and the dissociation constants that we measured were 2.04 and 4.7 μM, respectively, following again the same trend seen in the thermal melt assay (Figure 2C, Table 1). Affinity for BRD9 was lost when we synthesized compound **7e** which carried a bromine function at the meta′ position and an ethoxy substituent at the ortho position, suggesting that the longer and bulkier group probably affects rotation of the 6-aryl ring with respect to the core 9*H*-purine-2-amine fold.

In order to verify the mode of interaction of the 9*H*-purine core within the BRD acetyllysine binding cavity, we crystallized and determined the complexes of compound **7d** with the

DOI: 10.1021/jm501893k
J. Med. Chem. 2015, 58, 2718−2736

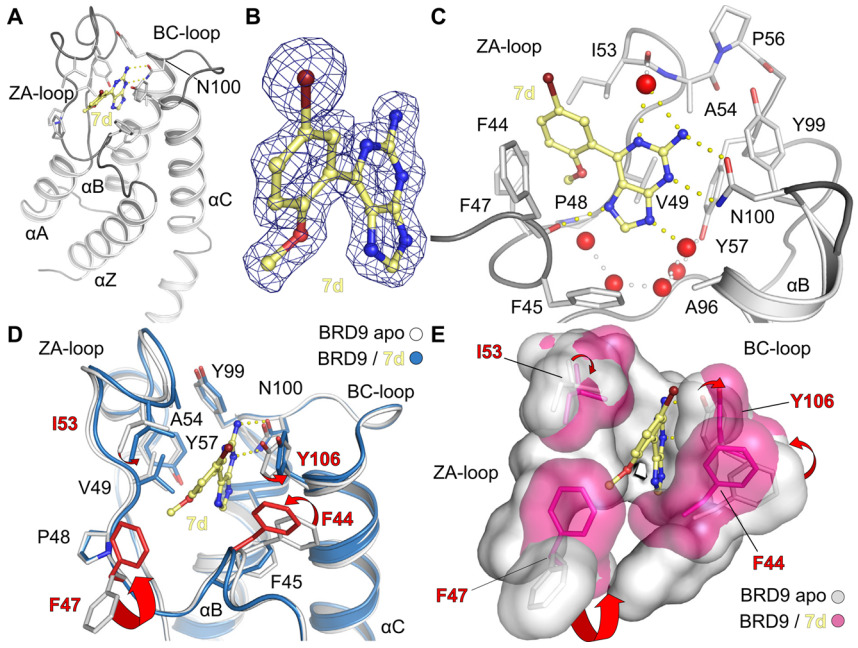

Figure 3. Induced fit binding of 9*H*-purines to BRD9. (A) Overall fold of BRD9/**7d** complex. (B) $2F_cF_o$ map of **7d** in complex with BRD9 contoured at 2σ. (C) **7d** occupies the acetyllysine binding cavity of the bromodomain module initiating direct interactions with the conserved asparagine (N100) and packing onto the ZA-loop hydrophobic backbone (F44, F47, I53, A54, P56, Y57). The conserved water network is preserved in the structure, and the ligand initiates hydrogen bonds that further stabilize binding. Notably the ligand engages a water molecule located on the top of the BRD cavity in a network of hydrogen bonds to the backbone of I53. (D) Binding of **7d** to BRD9 results in a distinct rearrangement of the BRD fold. Residues on both sides of the ligand shift toward it, forming an induced-fit pocket with F47 rotating 120° capping the channel found in the apo BRD9 structure at the front of the ZA-loop. (E) Surface view of the side chain rearrangement described in (C) highlighting the induced pocket upon binding of **7d** to BRD9. The model and structure factors of the BRD9/**7d** complex shown have been deposited to the PDB with ascension code 4XY8.

bromodomain of BRD9 and the first bromodomain of BRD4. The ligand was found in both cases to occupy the acetyllysine recognition pocket (Figure 3A and Supporting Information Figure 2A) and was clearly defined in the electron density map (Figure 3B and Supporting Information Figure 2B). Compound **7d** directly engaged, via the primary amine function as well as the nitrogen at position 3, the conserved asparagine in both structures (Asn100 in BRD9; Asn140 in BRD4(1)) and was additionally held in place via a number of hydrogen bonds to the protein backbone and the network of conserved water molecules previously described[76] (Figure 3C and Supporting Information Figure 2C). Notably, compound **7d** initiated hydrogen bonds to a water molecule located on top of the BRD cavity, which in turn linked the ligand to the top of the ZA-loop, either to the carbonyl of Ile53 (in the case of BRD9) or Asn93 (in the case of BRD4(1)). This tight network of interactions explains the potency of this compound for BRDs. The mode of interaction is similar to that observed before for triazolothienodiazepine complexes such as (+)-JQ1, with the five-membered ring of the purine system acting as the acetyllysine mimetic moiety, superimposing well with the methyltriazolo ring of (+)-JQ1 (Supporting Information Figure 2D) while the bromomethoxyphenyl substituent of **7d** stacks well between the ZA-loop Leu92 and the ZA-channel's Phe81/Pro82 of BRD4(1) (Supporting Information Figure 2E). Consistent with our induced fit computational models of binding of **2a** to BRD9, superimposition of the BRD9/**7d** complex to the apo structure of BRD9 (PDB code 3HME)[15] revealed rotations of the side chains of Phe47 and Phe44 while the top of the ZA loop collapsed toward the ligand (Figure 3D,E), resulting in an unprecedented induced fit pocket of BRD9. Particularly the side chain of Phe47 rotated 120°, thus blocking the ZA-channel of the protein resulting in a steric bulk around compound **7d**. On the basis of our thermodynamic measurements showing high entropic contributions to binding (Table 2), we concluded that all compounds in this subseries (**7a**–**d**) should be inducing a rearrangement of the binding cavity residues of BRD9 upon binding to the acetyllysine site. Intriguingly as the substituent size increases, the affinity also increases as exemplified by the determined dissociation constants, with the chloro analogue (**7c**) exhibiting a dissociation constant of 297 nM against BRD9 while the bromo analogue (**7d**) is slightly weaker (397 nM against BRD9; 4.65 μM against BRD4(1)). However, the structural rearrangement that we observed was unique to BRD9; the structure of compound **7d** in complex with the first bromodomain of BRD4 did not reveal any rearrangements of the acetyllysine binding cavity as the inhibitor packed between Trp81 and Leu92 of the ZA-loop (Supporting Information Figure 2D,E). It is tempting to speculate that the observed increase in entropic contributions within the series of compounds **7a**–**d** measured by ITC, following the increase in the halide substituent size, is associated with the side chain rearrangement observed by docking as well as the crystal structure of compound **7d** with the bromodomain of BRD9. However, entropy changes may be due to a number of factors, such as release of water molecules, therefore making further interpretation of the small data set obtained very difficult.

We next questioned whether the primary amine function at position 2 of the 9*H*-purine core scaffold is necessary for binding to bromodomains. First we substituted the amine with a chlorine group (compound **8a**, Figure 4A) while retaining the

DOI: 10.1021/jm501893k
J. Med. Chem. 2015, 58, 2718−2736

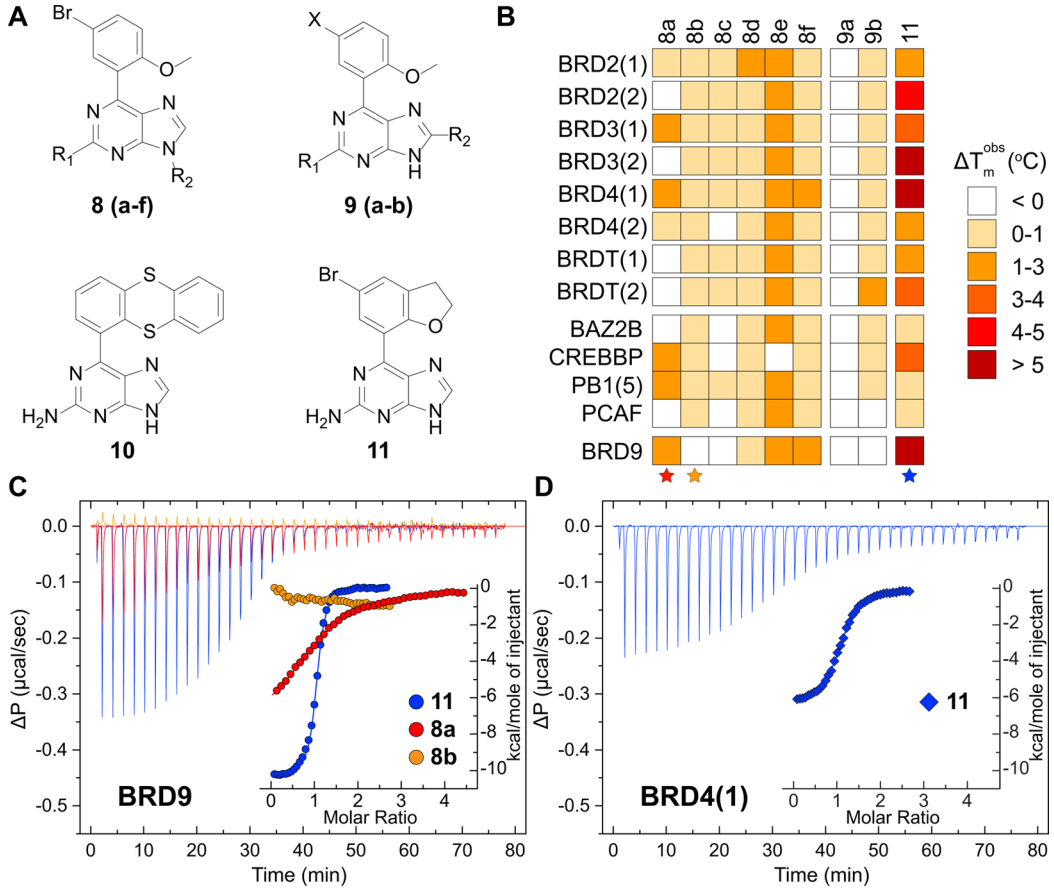

Figure 4. BRD pocket SAR. (A) Compounds designed to probe the acetyllysine mimetic character of the purine scaffold, disrupting interactions (N9-methyl analogues) or reaching deeper into the acetyllysine cavity (8-methyl analogues). (B) Thermal shift assay against human bromodomains. Compound **10** was heavily colored and interfered with the assay. Thermal shifts are color-coded as indicated in the inset. Compounds highlighted with a colored star were further validated as shown in (C)/(D). (C) Substitution of the primary amine group to a hydroxyl (compound **8a**) impairs binding toward BRD9 as demonstrated by ITC experiments, while cyclization of the aromatic substituent results in enhanced potency (compound **11**). The inset shows the normalized binding enthalpies corrected for the heat of protein dilution as a function of binding site saturation (symbols as indicated in the figure). Solid lines represent a nonlinear least-squares fit using a single-site binding model. (D) Isothermal titration calorimetry validation of compound **11** binding to BRD4(1) showing raw injection heats for titrations of protein into compound. Data have been corrected and displayed as described in (C). All ITC titrations were carried out in 50 mM HEPES, pH 7.5 (at 25 °C), 150 mM NaCl, and 15 °C while stirring at 1000 rpm.

6-(5-bromo-2-methoxyphenyl) substitution, resulting in loss of affinity toward all BRDs in our panel (Figure 4B). In the case of BRD9 we confirmed this observation by performing an isothermal titration calorimetry measurement which yielded a K_d of 7.9 μM (Figure 4C). As with compounds from previous series, methyl substitution at position 9 completely abolished bromodomain binding (compound **8b**, Figure 4A), measured by both thermal melt (Figure 4B) and ITC assays in the case of BRD9 (Figure 4C); larger substituents (compound **8c**) could not be tolerated suggesting that the core scaffold retained its pose within the bromodomain binding cavity. Hydroxy substitution at position 2 while retaining a 6-(5-halide-2-methoxyphenyl) substituent (compounds **8d**–**f**) had variable effects on the 9*H*-purine affinity toward BRDs. Moreover, fluoro (**8d**) and bromo (**8f**) substituted compounds lost affinity across the panel, while the chloro-substituted compound (**8e**) promiscuously bound to most bromodomains in the ΔT_m assay, albeit weaker than its primary amine analogue **7c** (Figure 4A,B), thus suggesting that the interactions initiated by the hydroxyl group and the conserved asparagine (Asn100 in BRD9; Asn140 in BRD4(1)) are not favored over the primary amine.

The 9*H*-purine crystal structure complexes that we obtained with the bromodomains of BRD9 and BRD4(1) highlighted the failure of the ligand to insert deep inside the bromodomain cavity, thus not replacing the conserved network of water molecules. In an attempt to reach deeper within the cavity, we synthesized compounds **9a** and **9b**, introducing a methyl group at position 8 of the 9*H*-purine core. The low solubility of compound **9a** did not allow for any measurements, but compound **9b** exhibited very low affinity for all bromodomains in our panel with the exception of BRDT(2) (ΔT_m of 2.9 °C), suggesting that substitution at this position of the 9*H*-purine core in the absence of a 2-amine function cannot be tolerated and these compounds could not displace the conserved water molecule network deep inside the bromodomain pocket. Our synthetic efforts to insert a fluorine atom at position 8 through a C-8 electrophilic fluorination on the bis(tetrahydropyran-2-yl)-protected derivative of **2a**, following a reported metalation–fluorination reaction with *N*-fluorobenzenesulfonimide,[78] were also unsuccessful; we observed formation of the corresponding 8-phenylsulfonyl product instead of the 8-fluoro derivative, similar to reported work done by Roy and co-workers,[79] even under heterogeneous conditions.

DOI: 10.1021/jm501893k
J. Med. Chem. 2015, 58, 2718–2736

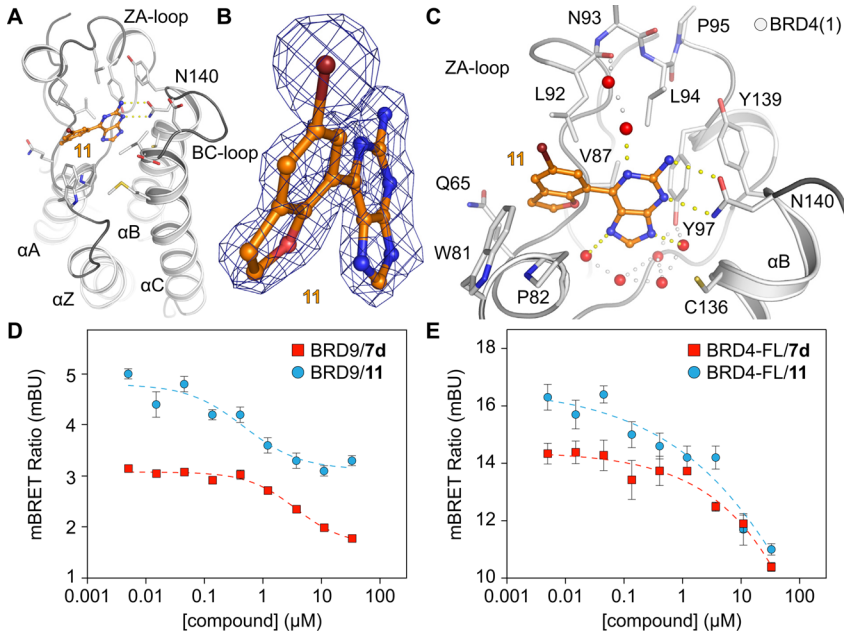

Figure 5. Complex of compound **11** and 9*H*-purine activity in cells. (A) Overview of the complex of compound **11** with the first bromodomain of BRD4. The ligand retained the acetyllysine mimetic pose that was observed in the case of **7d**. (B) Compound **11** F_cF_o omit map from the BRD4(1)/**11** complex contoured at 2σ. (C) Detail of compound **11** biding to BRD4(1) demonstrating the acetyllysine mimetic binding mode, initiating interactions with the conserved asparagine (N140), and packing between the ZA-loop L92 and the ZA-channel W81 while retaining the network of conserved water interactions. The model and structure factors of the BRD4(1)/**11** complex shown in panels A, B, and C have been deposited to the PDB with ascension code 4XYA. (D) Titration of compounds **7d** and **11** into HEK293 cells transfected with NanoLuc-fused bromodomain of BRD9 and Halo-tagged histone H3.3. The ligands disrupt the histone/BRD9 interaction with an apparent IC_{50} of 3.5 μM (**7d**) and 480 nM (**11**), resulting in loss of signal due to separation of the BRD9-histone complex. (E) Titration of compounds **7d** and **11** into HEK293 cells transfected with NanoLuc-fused full length BRD4 (UniProt code O60885) and Halo-tagged histone H3.3. Although the ligands gradually disrupt the BRD4-FL/H3.3 interaction, they fail to elicit the same effect as in the case of BRD9 in the concentration range tested.

Our structural insight suggested that augmentation of the 6-(5-halide-2-methoxyphenyl) substituent would take a toll on BRD9, as it would force the structure toward an apo-like conformation, sterically pushing Phe47 toward the apo-conformation of BRD9, while it should not affect binding to BET bromodomains which contained an open channel between Trp81 and Leu92 (Figure 3E and Supporting Information Figure 2E) . To test this hypothesis, we synthesized compound **10** (Figure 4A) and tested its ability to bind to human BRDs. Unfortunately its bright yellow color and low solubility did not allow for further validation. We therefore decided to increase the size of the substituent found in **7d** by cyclizing the 2-methoxyphenyl ring into a 2,3-dihydrobenzofuran-7-yl while retaining the bromo function at position 5. We tested the resulting compound **11** in the ΔT_m assay against the panel of bromodomains and observed increased temperature shifts among BET BRDs (between 1.7 and 5.4 °C) together with a remarkable increase in the case of BRD9 (6.5 °C). To verify this observation, we performed isothermal titration calorimetry measurements and obtained a dissociation constant of 278 nM for BRD9 (Figure 4C) while BRD4(1) binding resulted in a much weaker affinity (1.4 μM) (Figure 4D). Notably the entropic contribution of compound **11** binding to BRD9 was comparable to compound **7d** for both BRD9 and BRD4(1), and thus we speculated that a similar rearrangement should be taking place upon binding to the bromodomain of BRD9.

In order to test our hypothesis that compound **11** binding would also result in structural rearrangement of the bromodomain binding cavity of BRD9, in a similar way to compound **7d**, while not affecting the cavity of BRD4(1), we attempted to determine the crystal structures of this compound in complex with these two bromodomains. Compound **11** readily crystallized with BRD4(1) and was found to occupy the acetyllysine binding cavity of the bromodomain (Figure 5A) and was very well-defined in the density (Figure 5B) despite its weaker binding affinity of 1.37 μM toward BRD4(1) (Table 1). The ligand was found to directly interact with the conserved asparagine (Asn140) as well as with the conserved network of water molecules while packing between the ZA-channel tryptophan (Trp81) and the ZA-loop leucine (Leu92) (Figure 5C). Our efforts however to obtain a BRD9/**11** complex did not yield diffracting quality crystals suitable for structure determination, and as such, we employed computational methods to account for its binding to BRD9. Rigid docking into the BRD9/**7d** complex structure resulted in a conformation similar to that observed with compound **7d**, with the ligand engaging the conserved asparagine via its primary amine function and the 6-aryl-substituted ring packing between the ZA-loop Ile53 and Phe44 (Supporting Information Figure 3A). We then performed induced-fit docking employing the algorithms previously described for purine fragments using the complex of BRD9/**7d** as starting point and obtained a pose whereby the 2-amine function inverted and inserted in the BRD pocket, without any changes in the surrounding side chains of Phe44, Phe47, Ile53, and Tyr106 (Supporting Information Figure 3B). Intrigued by this finding, we performed another induced fit docking experiment, starting with the BRD9 apo structure and allowing residues to freely move in the presence of the ligand. We observed a similar set of side chain rearrangement within the BRD9 acetyllysine cavity, including

DOI: 10.1021/jm501893k
J. Med. Chem. 2015, 58, 2718−2736

a rotation of Phe47 resulting in capping of the binding groove, accompanied by repositioning of Phe44 from helix C and Ile53 from the ZA-loop (Supporting Information Figure 3C). We therefore concluded that the 2-amine-9*H*-purine scaffolds that we developed can induce a closed pocket within the bromodomain of BRD9 resulting in tight binding, without at the same time exhibiting high affinity for BRD4(1) or other BET family members. Indeed, we determined the dissociation constants for binding to BET domains employing ITC and found that both compounds **7d** and **11** exhibited low micromolar affinities (1.4−4.6 μM) correlating well with the higher thermal shifts observed (Supporting Information Table S1), while retaining higher affinity against the bromodomain of BRD9 (Supporting Information Figure 4 and Tables 2 and 3).

Having obtained a small window of selectivity over BRD4, we wanted to verify that the 2-amine-9*H*-purine scaffolds that we developed are in fact active in a cellular environment and can perturb the interaction of BRD9 with acetylated histones. Previous studies have established that potent compounds that competitively bind to the acetyllysine binding cavity of BET proteins can displace the entire protein from chromatin in fluorescence recovery after photobleaching (FRAP) assays,[23,35,77] while larger BRD-containing proteins that contain in addition multiple reader domains are harder to fully displace; in the case of CREBBP this was solved by creating an artificial GFP-fusion construct that contained three BRD modules of CREBBP and a nuclear localization signal.[38] BRD9 is part of the large SWI/SNF complex,[49] and its bromodomain has been shown to bind to acetylated histone H3 peptides.[15] We speculated that 9*H*-purines should be able to competitively displace the bromodomain of BRD9 from chromatin and constructed a bioluminescence resonance energy transfer (BRET) system that combined NanoLuc luciferase fusions of the BRD9 bromodomain (Supporting Information Figure 5A) or full length BRD4 and Halo-tagged histone H3.3 as BRET pairs. This assay is an excellent tool to quantify protein−ligand interactions in a cellular system[80] and has recently been used to determine cellular IC_{50} values for the inhibition of the histone−bromodomain interaction in the case of BRPF1 using a 1,3-dimethylbenzimidazolone scaffold.[42] First we established by fluorescence microscopy that Halo-tagged histone H3.3 is readily incorporated into chromatin (Supporting Information Figure 5B). We then performed dose−response experiments and demonstrated the NanoLuc-BRD9 bromodomain was readily displaced from chromatin by compounds **7d** and **11** with cellular IC_{50} values of 3.5 ± 0.11 μM and 477 ± 194 nM, respectively (Figure 5D), in agreement with the in vitro affinities determined by ITC (Table 2). In contrast, full-length BRD4 was not completely displaced in this assay up to concentrations of 33 μM of both compounds (Figure 5E), suggesting that the compounds retained the in vitro selectivity toward BRD9 in this cellular system. We further examined the toxicity of compound **11** toward HEK293 cells, using cell viability in the presence of the compound in the concentration regime of our BRET experiments as a readout and did not observe any cytotoxicty (Supporting Information Figure 5C), suggesting that this compound can be used in cellular systems to target BRD9/Kac interactions without affecting BRD4/Kac interactions or causing any cytotoxic responses.

CONCLUSION

We have described here a structure-guided approach to identify inhibitors for diverse BRDs starting from small fragment-like 9*H*-purine scaffolds. Through structure−activity relationship we established compounds **7d** and **11** and characterized them as nanomolar binders for the BRD of BRD9 while retaining weak in vitro activity against the first bromodomain of BRD4. These compounds are not cytotoxic at concentrations up to 33 μM in a HEK293 system and can competitively displace the BRD9 bromodomain from chromatin while failing to displace full length human BRD4 at the same concentration range in bioluminescence proximity assays, despite the fact that the in vitro affinity difference for these two proteins is not large. Importantly, compound **7d** induces structural rearrangement on the acetyllysine binding cavity of BRD9 resulting in an unprecedented cavity shape which accommodates this scaffold, explaining the higher affinity toward this protein, while docking studies suggest that compound **11** elicits the same type of structural rearrangement. The 9*H*-purine scaffold therefore offers a simple template that can be used to generate initial tools that will no doubt prove useful in interrogating the biology of bromodomains beyond the BET subfamily, such as BRD9, which have not attracted attention until now, avoiding cross-reactivity with BET bromodomains.

ASSOCIATED CONTENT

Supporting Information

Figures showing alternative docking of **2a**, binding of **7d** to BRD4(1), docking of **11** to BRD9, and binding of **7d** and **11** to BET bromodomains and a file in xlsx format listing ΔT_m shifts of compounds. This material is available free of charge via the Internet at http://pubs.acs.org.

Accession Codes

The models and structure factors have been deposited in the PDB with accession codes 4XY8, 4XY9, 4XYA.

AUTHOR INFORMATION

Corresponding Authors

*G.B.: e-mail, bifulco@unisa.it; phone, +39 (0) 89 969741; fax, +39 (0) 89 962804.

*I.B.: e-mail, brunoin@unisa.it; phone, +39 (0) 89 969743; fax, +39 (0) 89 962804.

*P.F.: e-mail, panagis.filippakopoulos@sgc.ox.ac.uk; phone, +44 (0) 1865 617759; fax, +44 (0) 1865 617575.

Author Contributions

#S.P. and M.S. contributed equally.

The manuscript was written through contributions of all authors. All authors have given approval to the final version of the manuscript.

Notes

The authors declare no competing financial interest.

ACKNOWLEDGMENTS

Financial support by the University of Salerno is gratefully acknowledged. The authors also acknowledge the use of the instrument facilities of the Centre of Competence in Diagnostics and Molecular Pharmaceutics supported by Regione Campania (Italy) through POR funds, an Associazione Italiana Ricerca sul Cancro (AIRC) fellowship (G.L.), and Grant IG 2012-IG_12777 (G.B.). The SGC is a registered charity (No. 1097737) that receives funds from AbbVie, Bayer, Boehringer Ingelheim, and Genome Canada through Ontario Genomics Institute Grant OGI-055, GlaxoSmithKline, Janssen, Lilly Canada, the Novartis Research Foundation, the Ontario Ministry of Economic Development and Innovation, Pfizer,

DOI: 10.1021/jm501893k
J. Med. Chem. 2015, 58, 2718−2736

Takeda, and the Wellcome Trust (Grant 092809/Z/10/Z). P.F. and S.P. are supported by a Wellcome Trust Career Development Fellowship (Grant 095751/Z/11/Z).

■ ABBREVIATIONS USED

ATAD2, ATPase family, AAA domain containing 2; BAZ2B, bromodomain adjacent to zinc finger domain 2B; BET, bromo and extra C-terminal domain protein; BRD, bromodomain; BRD2, bromodomain containing protein 2; BRD3, bromodomain containing protein 3; BRD4, bromodomain containing protein 4; BRD7, bromodomain containing protein 7; BRD9, bromodomain containing protein 9; BRDT, bromodomain testis-specific protein; BRET, bioluminescence resonance energy transfer; BRPF1, bromodomain and PHD finger containing 1; CREBBP, cAMP response element binding protein (CREB) binding protein; Kac, *N*-ε-acetyllysine; PB1, polybromo-containing protein; PCAF, P300/CBP-associated factor; TBAF, tetrabutylammonium fluoride

■ REFERENCES

(1) Bernstein, B. E.; Meissner, A.; Lander, E. S. The mammalian epigenome. *Cell* **2007**, *128*, 669−681.
(2) Strahl, B. D.; Allis, C. D. The language of covalent histone modifications. *Nature* **2000**, *403*, 41−45.
(3) Choudhary, C.; Kumar, C.; Gnad, F.; Nielsen, M. L.; Rehman, M.; Walther, T. C.; Olsen, J. V.; Mann, M. Lysine acetylation targets protein complexes and co-regulates major cellular functions. *Science* **2009**, *325*, 834−840.
(4) Filippakopoulos, P.; Knapp, S. The bromodomain interaction module. *FEBS Lett.* **2012**, *586*, 2692−2704.
(5) Tamkun, J. W.; Deuring, R.; Scott, M. P.; Kissinger, M.; Pattatucci, A. M.; Kaufman, T. C.; Kennison, J. A. brahma: a regulator of *Drosophila* homeotic genes structurally related to the yeast transcriptional activator SNF2/SWI2. *Cell* **1992**, *68*, 561−572.
(6) Li, Y.; Wen, H.; Xi, Y.; Tanaka, K.; Wang, H.; Peng, D.; Ren, Y.; Jin, Q.; Dent, S. Y.; Li, W.; Li, H.; Shi, X. AF9 YEATS domain links histone acetylation to DOT1L-mediated H3K79 methylation. *Cell* **2014**, *159*, 558−571.
(7) Yang, X. J.; Ogryzko, V. V.; Nishikawa, J.; Howard, B. H.; Nakatani, Y. A p300/CBP-associated factor that competes with the adenoviral oncoprotein E1A. *Nature* **1996**, *382*, 319−324.
(8) Dhalluin, C.; Carlson, J. E.; Zeng, L.; He, C.; Aggarwal, A. K.; Zhou, M. M. Structure and ligand of a histone acetyltransferase bromodomain. *Nature* **1999**, *399*, 491−496.
(9) Jacobson, R. H.; Ladurner, A. G.; King, D. S.; Tjian, R. Structure and function of a human TAFII250 double bromodomain module. *Science* **2000**, *288*, 1422−1425.
(10) Venturini, L.; You, J.; Stadler, M.; Galien, R.; Lallemand, V.; Koken, M. H.; Mattei, M. G.; Ganser, A.; Chambon, P.; Losson, R.; de The, H. TIF1gamma, a novel member of the transcriptional intermediary factor 1 family. *Oncogene* **1999**, *18*, 1209−1217.
(11) Cavellan, E.; Asp, P.; Percipalle, P.; Farrants, A. K. The WSTF-SNF2h chromatin remodeling complex interacts with several nuclear proteins in transcription. *J. Biol. Chem.* **2006**, *281*, 16264−16271.
(12) Trotter, K. W.; Archer, T. K. The BRG1 transcriptional coregulator. *Nucl. Recept Signaling* **2008**, *6*, e004.
(13) Xue, Y.; Canman, J. C.; Lee, C. S.; Nie, Z.; Yang, D.; Moreno, G. T.; Young, M. K.; Salmon, E. D.; Wang, W. The human SWI/SNF-B chromatin-remodeling complex is related to yeast rsc and localizes at kinetochores of mitotic chromosomes. *Proc. Natl. Acad. Sci. U.S.A.* **2000**, *97*, 13015−13020.
(14) Wu, S. Y.; Chiang, C. M. The double bromodomain-containing chromatin adaptor Brd4 and transcriptional regulation. *J. Biol. Chem.* **2007**, *282*, 13141−13145.
(15) Filippakopoulos, P.; Picaud, S.; Mangos, M.; Keates, T.; Lambert, J. P.; Barsyte-Lovejoy, D.; Felletar, I.; Volkmer, R.; Muller, S.; Pawson, T.; Gingras, A. C.; Arrowsmith, C. H.; Knapp, S. Histone recognition and large-scale structural analysis of the human bromodomain family. *Cell* **2012**, *149*, 214−231.
(16) Belkina, A. C.; Denis, G. V. BET domain co-regulators in obesity, inflammation and cancer. *Nat. Rev. Cancer* **2012**, *12*, 465−477.
(17) Lamonica, J. M.; Deng, W.; Kadauke, S.; Campbell, A. E.; Gamsjaeger, R.; Wang, H.; Cheng, Y.; Billin, A. N.; Hardison, R. C.; Mackay, J. P.; Blobel, G. A. Bromodomain protein Brd3 associates with acetylated GATA1 to promote its chromatin occupancy at erythroid target genes. *Proc. Natl. Acad. Sci. U.S.A.* **2011**, *108*, E159−168.
(18) Shi, J.; Wang, Y.; Zeng, L.; Wu, Y.; Deng, J.; Zhang, Q.; Lin, Y.; Li, J.; Kang, T.; Tao, M.; Rusinova, E.; Zhang, G.; Wang, C.; Zhu, H.; Yao, J.; Zeng, Y. X.; Evers, B. M.; Zhou, M. M.; Zhou, B. P. Disrupting the interaction of BRD4 with diacetylated Twist suppresses tumorigenesis in basal-like breast cancer. *Cancer Cell* **2014**, *25*, 210−225.
(19) Huang, B.; Yang, X. D.; Zhou, M. M.; Ozato, K.; Chen, L. F. Brd4 coactivates transcriptional activation of NF-kappaB via specific binding to acetylated RelA. *Mol. Cell. Biol.* **2009**, *29*, 1375−1387.
(20) Schroder, S.; Cho, S.; Zeng, L.; Zhang, Q.; Kaehlcke, K.; Mak, L.; Lau, J.; Bisgrove, D.; Schnolzer, M.; Verdin, E.; Zhou, M. M.; Ott, M. Two-pronged binding with bromodomain-containing protein 4 liberates positive transcription elongation factor b from inactive ribonucleoprotein complexes. *J. Biol. Chem.* **2012**, *287*, 1090−1099.
(21) Rahman, S.; Sowa, M. E.; Ottinger, M.; Smith, J. A.; Shi, Y.; Harper, J. W.; Howley, P. M. The Brd4 extraterminal domain confers transcription activation independent of pTEFb by recruiting multiple proteins, including NSD3. *Mol. Cell. Biol.* **2011**, *31*, 2641−2652.
(22) Bres, V.; Yoh, S. M.; Jones, K. A. The multi-tasking P-TEFb complex. *Curr. Opin. Cell Biol.* **2008**, *20*, 334−340.
(23) Filippakopoulos, P.; Qi, J.; Picaud, S.; Shen, Y.; Smith, W. B.; Fedorov, O.; Morse, E. M.; Keates, T.; Hickman, T. T.; Felletar, I.; Philpott, M.; Munro, S.; McKeown, M. R.; Wang, Y.; Christie, A. L.; West, N.; Cameron, M. J.; Schwartz, B.; Heightman, T. D.; La Thangue, N.; French, C. A.; Wiest, O.; Kung, A. L.; Knapp, S.; Bradner, J. E. Selective inhibition of BET bromodomains. *Nature* **2010**, *468*, 1067−1073.
(24) Nicodeme, E.; Jeffrey, K. L.; Schaefer, U.; Beinke, S.; Dewell, S.; Chung, C. W.; Chandwani, R.; Marazzi, I.; Wilson, P.; Coste, H.; White, J.; Kirilovsky, J.; Rice, C. M.; Lora, J. M.; Prinjha, R. K.; Lee, K.; Tarakhovsky, A. Suppression of inflammation by a synthetic histone mimic. *Nature* **2010**, *468*, 1119−1123.
(25) Filippakopoulos, P.; Knapp, S. Targeting bromodomains: epigenetic readers of lysine acetylation. *Nat. Rev. Drug Discovery* **2014**, *13*, 337−356.
(26) Hewings, D. S.; Wang, M.; Philpott, M.; Fedorov, O.; Uttarkar, S.; Filippakopoulos, P.; Picaud, S.; Vuppusetty, C.; Marsden, B.; Knapp, S.; Conway, S. J.; Heightman, T. D. 3,5-Dimethylisoxazoles act as acetyl-lysine-mimetic bromodomain ligands. *J. Med. Chem.* **2011**, *54*, 6761−6770.
(27) McKeown, M. R.; Shaw, D. L.; Fu, H.; Liu, S.; Xu, X.; Marineau, J. J.; Huang, Y.; Zhang, X.; Buckley, D. L.; Kadam, A.; Zhang, Z.; Blacklow, S. C.; Qi, J.; Zhang, W.; Bradner, J. E. Biased multicomponent reactions to develop novel bromodomain inhibitors. *J. Med. Chem.* **2014**, *57*, 9019−9027.
(28) Fish, P. V.; Filippakopoulos, P.; Bish, G.; Brennan, P. E.; Bunnage, M. E.; Cook, A. S.; Federov, O.; Gerstenberger, B. S.; Jones, H.; Knapp, S.; Marsden, B.; Nocka, K.; Owen, D. R.; Philpott, M.; Picaud, S.; Primiano, M. J.; Ralph, M. J.; Sciammetta, N.; Trzupek, J. D. Identification of a chemical probe for bromo and extra C-terminal bromodomain inhibition through optimization of a fragment-derived hit. *J. Med. Chem.* **2012**, *55*, 9831−9837.
(29) Chung, C. W.; Dean, A. W.; Woolven, J. M.; Bamborough, P. Fragment-based discovery of bromodomain inhibitors part 1: inhibitor binding modes and implications for lead discovery. *J. Med. Chem.* **2012**, *55*, 576−586.
(30) Vidler, L. R.; Filippakopoulos, P.; Fedorov, O.; Picaud, S.; Martin, S.; Tomsett, M.; Woodward, H.; Brown, N.; Knapp, S.; Hoelder, S. Discovery of novel small-molecule inhibitors of BRD4 using structure-based virtual screening. *J. Med. Chem.* **2013**, *56*, 8073−8088.

DOI: 10.1021/jm501893k
J. Med. Chem. 2015, 58, 2718−2736

(31) Zhao, L.; Cao, D.; Chen, T.; Wang, Y.; Miao, Z.; Xu, Y.; Chen, W.; Wang, X.; Li, Y.; Du, Z.; Xiong, B.; Li, J.; Xu, C.; Zhang, N.; He, J.; Shen, J. Fragment-based drug discovery of 2-thiazolidinones as inhibitors of the histone reader BRD4 bromodomain. *J. Med. Chem.* **2013**, *56*, 3833−3851.
(32) Lucas, X.; Wohlwend, D.; Hugle, M.; Schmidtkunz, K.; Gerhardt, S.; Schule, R.; Jung, M.; Einsle, O.; Gunther, S. 4-Acyl pyrroles: mimicking acetylated lysines in histone code reading. *Angew. Chem., Int. Ed.* **2013**, *52*, 14055−14059.
(33) Fedorov, O.; Lingard, H.; Wells, C.; Monteiro, O. P.; Picaud, S.; Keates, T.; Yapp, C.; Philpott, M.; Martin, S. J.; Felletar, I.; Marsden, B. D.; Filippakopoulos, P.; Muller, S.; Knapp, S.; Brennan, P. E. [1,2,4]Triazolo[4,3-a]phthalazines: inhibitors of diverse bromodomains. *J. Med. Chem.* **2014**, *57*, 462−476.
(34) Bamborough, P.; Diallo, H.; Goodacre, J. D.; Gordon, L.; Lewis, A.; Seal, J. T.; Wilson, D. M.; Woodrow, M. D.; Chung, C. W. Fragment-based discovery of bromodomain inhibitors part 2: optimization of phenylisoxazole sulfonamides. *J. Med. Chem.* **2012**, *55*, 587−596.
(35) Picaud, S.; Da Costa, D.; Thanasopoulou, A.; Filippakopoulos, P.; Fish, P. V.; Philpott, M.; Fedorov, O.; Brennan, P.; Bunnage, M. E.; Owen, D. R.; Bradner, J. E.; Taniere, P.; O'Sullivan, B.; Muller, S.; Schwaller, J.; Stankovic, T.; Knapp, S. PFI-1, a highly selective protein interaction inhibitor, targeting BET Bromodomains. *Cancer Res.* **2013**, *73*, 3336−3346.
(36) Vidler, L. R.; Brown, N.; Knapp, S.; Hoelder, S. Druggability analysis and structural classification of bromodomain acetyl-lysine binding sites. *J. Med. Chem.* **2012**, *55*, 7346−7359.
(37) SGC. GSK2801: A Selective Chemical Probe for BAZ2B/A Bromodomains. http://www.thesgc.org/chemical-probes/GSK2801.
(38) Hay, D. A.; Fedorov, O.; Martin, S.; Singleton, D. C.; Tallant, C.; Wells, C.; Picaud, S.; Philpott, M.; Monteiro, O. P.; Rogers, C. M.; Conway, S. J.; Rooney, T. P.; Tumber, A.; Yapp, C.; Filippakopoulos, P.; Bunnage, M. E.; Muller, S.; Knapp, S.; Schofield, C. J.; Brennan, P. E. Discovery and optimization of small-molecule ligands for the CBP/p300 bromodomains. *J. Am. Chem. Soc.* **2014**, *136*, 9308−9319.
(39) Chaikuad, A.; Petros, A. M.; Fedorov, O.; Xu, J.; Knapp, S. Structure-based approaches towards identification of fragments for the low-druggability ATAD2 bromodomain. *Med. Chem. Commun.* **2014**, *5*, 1843−1848.
(40) Harner, M. J.; Chauder, B. A.; Phan, J.; Fesik, S. W. Fragment-Based Screening of the Bromodomain of ATAD2. *J. Med. Chem.* **2014**, *57*, 9687−9692.
(41) Ferguson, F. M.; Fedorov, O.; Chaikuad, A.; Philpott, M.; Muniz, J. R.; Felletar, I.; von Delft, F.; Heightman, T.; Knapp, S.; Abell, C.; Ciulli, A. Targeting low-druggability bromodomains: fragment based screening and inhibitor design against the BAZ2B bromodomain. *J. Med. Chem.* **2013**, *56*, 10183−10187.
(42) Demont, E. H.; Bamborough, P.; Chung, C. W.; Craggs, P. D.; Fallon, D.; Gordon, L. J.; Grandi, P.; Hobbs, C. I.; Hussain, J.; Jones, E. J.; Le Gall, A.; Michon, A. M.; Mitchell, D. J.; Prinjha, R. K.; Roberts, A. D.; Sheppard, R. J.; Watson, R. J. 1,3-Dimethyl benzimidazolones are potent, selective inhibitors of the BRPF1 bromodomain. *ACS Med. Chem. Lett.* **2014**, *5*, 1190−1195.
(43) Ciceri, P.; Muller, S.; O'Mahony, A.; Fedorov, O.; Filippakopoulos, P.; Hunt, J. P.; Lasater, E. A.; Pallares, G.; Picaud, S.; Wells, C.; Martin, S.; Wodicka, L. M.; Shah, N. P.; Treiber, D. K.; Knapp, S. Dual kinase-bromodomain inhibitors for rationally designed polypharmacology. *Nat. Chem. Biol.* **2014**, *10*, 305−312.
(44) Martin, M. P.; Olesen, S. H.; Georg, G. I.; Schonbrunn, E. Cyclin-dependent kinase inhibitor dinaciclib interacts with the acetyl-lysine recognition site of bromodomains. *ACS Chem. Biol.* **2013**, *8*, 2360−2365.
(45) Rosemeyer, H. The chemodiversity of purine as a constituent of natural products. *Chem. Biodiversity* **2004**, *1*, 361−401.
(46) U.S. Food and Drug Administration. http://www.fda.gov/ (accessed November 24, 2014).
(47) Gray, N. S.; Wodicka, L.; Thunnissen, A. M.; Norman, T. C.; Kwon, S.; Espinoza, F. H.; Morgan, D. O.; Barnes, G.; LeClerc, S.; Meijer, L.; Kim, S. H.; Lockhart, D. J.; Schultz, P. G. Exploiting chemical libraries, structure, and genomics in the search for kinase inhibitors. *Science* **1998**, *281*, 533−538.
(48) Legraverend, M.; Grierson, D. S. The purines: potent and versatile small molecule inhibitors and modulators of key biological targets. *Bioorg. Med. Chem.* **2006**, *14*, 3987−4006.
(49) Kadoch, C.; Hargreaves, D. C.; Hodges, C.; Elias, L.; Ho, L.; Ranish, J.; Crabtree, G. R. Proteomic and bioinformatic analysis of mammalian SWI/SNF complexes identifies extensive roles in human malignancy. *Nat. Genet.* **2013**, *45*, 592−601.
(50) Kang, J. U.; Koo, S. H.; Kwon, K. C.; Park, J. W.; Kim, J. M. Gain at chromosomal region 5p15.33, containing TERT, is the most frequent genetic event in early stages of non-small cell lung cancer. *Cancer Genet. Cytogenet.* **2008**, *182*, 1−11.
(51) Scotto, L.; Narayan, G.; Nandula, S. V.; Subramaniyam, S.; Kaufmann, A. M.; Wright, J. D.; Pothuri, B.; Mansukhani, M.; Schneider, A.; Arias-Pulido, H.; Murty, V. V. Integrative genomics analysis of chromosome 5p gain in cervical cancer reveals target over-expressed genes, including Drosha. *Mol. Cancer* **2008**, *7*, 58.
(52) Cleary, S. P.; Jeck, W. R.; Zhao, X.; Chen, K.; Selitsky, S. R.; Savich, G. L.; Tan, T. X.; Wu, M. C.; Getz, G.; Lawrence, M. S.; Parker, J. S.; Li, J.; Powers, S.; Kim, H.; Fischer, S.; Guindi, M.; Ghanekar, A.; Chiang, D. Y. Identification of driver genes in hepatocellular carcinoma by exome sequencing. *Hepatology* **2013**, *58*, 1693−1702.
(53) The Cancer Genome Atlas Research Network; Kandoth, C.; Schultz, N.; Cherniack, A. D.; Akbani, R.; Liu, Y.; Shen, H.; Robertson, A. G.; Pashtan, I.; Shen, R.; Benz, C. C.; Yau, C.; Laird, P. W.; Ding, L.; Zhang, W.; Mills, G. B.; Kucherlapati, R.; Mardis, E. R.; Levine, D. A. Integrated genomic characterization of endometrial carcinoma. *Nature* **2013**, *497*, 67−73.
(54) The Cancer Genome Atlas Research Network.. Comprehensive genomic characterization of squamous cell lung cancers. *Nature* **2012**, *489*, 519−525.
(55) Barbieri, C. E.; Baca, S. C.; Lawrence, M. S.; Demichelis, F.; Blattner, M.; Theurillat, J. P.; White, T. A.; Stojanov, P.; Van Allen, E.; Stransky, N.; Nickerson, E.; Chae, S. S.; Boysen, G.; Auclair, D.; Onofrio, R. C.; Park, K.; Kitabayashi, N.; MacDonald, T. Y.; Sheikh, K.; Vuong, T.; Guiducci, C.; Cibulskis, K.; Sivachenko, A.; Carter, S. L.; Saksena, G.; Voet, D.; Hussain, W. M.; Ramos, A. H.; Winckler, W.; Redman, M. C.; Ardlie, K.; Tewari, A. K.; Mosquera, J. M.; Rupp, N.; Wild, P. J.; Moch, H.; Morrissey, C.; Nelson, P. S.; Kantoff, P. W.; Gabriel, S. B.; Golub, T. R.; Meyerson, M.; Lander, E. S.; Getz, G.; Rubin, M. A.; Garraway, L. A. Exome sequencing identifies recurrent SPOP, FOXA1 and MED12 mutations in prostate cancer. *Nat. Genet.* **2012**, *44*, 685−689.
(56) Bosshard, H. R. Molecular recognition by induced fit: How fit is the concept? *News Physiol. Sci.* **2001**, *16*, 171−173.
(57) Rooney, T. P.; Filippakopoulos, P.; Fedorov, O.; Picaud, S.; Cortopassi, W. A.; Hay, D. A.; Martin, S.; Tumber, A.; Rogers, C. M.; Philpott, M.; Wang, M.; Thompson, A. L.; Heightman, T. D.; Pryde, D. C.; Cook, A.; Paton, R. S.; Muller, S.; Knapp, S.; Brennan, P. E.; Conway, S. J. A series of potent CREBBP bromodomain ligands reveals an induced-fit pocket stabilized by a cation-pi interaction. *Angew. Chem., Int. Ed.* **2014**, *53*, 6126−6130.
(58) Friesner, R. A.; Banks, J. L.; Murphy, R. B.; Halgren, T. A.; Klicic, J. J.; Mainz, D. T.; Repasky, M. P.; Knoll, E. H.; Shelley, M.; Perry, J. K.; Shaw, D. E.; Francis, P.; Shenkin, P. S. Glide: a new approach for rapid, accurate docking and scoring. 1. Method and assessment of docking accuracy. *J. Med. Chem.* **2004**, *47*, 1739−1749.
(59) Halgren, T. A.; Murphy, R. B.; Friesner, R. A.; Beard, H. S.; Frye, L. L.; Pollard, W. T.; Banks, J. L. Glide: a new approach for rapid, accurate docking and scoring. 2. Enrichment factors in database screening. *J. Med. Chem.* **2004**, *47*, 1750−1759.
(60) Friesner, R. A.; Murphy, R. B.; Repasky, M. P.; Frye, L. L.; Greenwood, J. R.; Halgren, T. A.; Sanschagrin, P. C.; Mainz, D. T. Extra precision glide: docking and scoring incorporating a model of hydrophobic enclosure for protein−ligand complexes. *J. Med. Chem.* **2006**, *49*, 6177−6196.

DOI: 10.1021/jm501893k
J. Med. Chem. 2015, 58, 2718−2736

(61) Sherman, W.; Day, T.; Jacobson, M. P.; Friesner, R. A.; Farid, R. Novel procedure for modeling ligand/receptor induced fit effects. *J. Med. Chem.* **2006**, *49*, 534−553.
(62) Sherman, W.; Beard, H. S.; Farid, R. Use of an induced fit receptor structure in virtual screening. *Chem. Biol. Drug Des.* **2006**, *67*, 83−84.
(63) Hocek, M.; Holy, A.; Votruba, I.; Dvorakova, H. Synthesis and cytostatic activity of substituted 6-phenylpurine bases and nucleosides: application of the Suzuki−Miyaura cross-coupling reactions of 6-chloropurine derivatives with phenylboronic acids. *J. Med. Chem.* **2000**, *43*, 1817−1825.
(64) Capek, P.; Vrabel, M.; Hasnik, Z.; Pohl, R.; Hocek, M. Aqueous-phase Suzuki−Miyaura cross-coupling reactions of free halopurine bases. *Synthesis* **2006**, 3515−3526.
(65) Matulis, D.; Kranz, J. K.; Salemme, F. R.; Todd, M. J. Thermodynamic stability of carbonic anhydrase: measurements of binding affinity and stoichiometry using ThermoFluor. *Biochemistry* **2005**, *44*, 5258−5266.
(66) Wiseman, T.; Williston, S.; Brandts, J. F.; Lin, L. N. Rapid measurement of binding constants and heats of binding using a new titration calorimeter. *Anal. Biochem.* **1989**, *179*, 131−137.
(67) Leslie, A. G. W.; Powell, H. *MOSFLM*, version 7.01; MRC Laboratory of Molecular Biology: Cambridge, U.K., 2007.
(68) Kabsch, W. Evaluation of single-crystal X-ray-diffraction data from a position-sensitive detector. *J. Appl. Crystallogr.* **1988**, *21*, 916−924.
(69) Kabsch, W. Automatic-indexing of rotation diffraction patterns. *J. Appl. Crystallogr.* **1988**, *21*, 67−71.
(70) Evans, P. *SCALA—Scale Together Multiple Observations of Reflections*, version 3.3.0; MRC Laboratory of Molecular Biology: Cambridge, U.K., 2007.
(71) McCoy, A. J.; Grosse-Kunstleve, R. W.; Storoni, L. C.; Read, R. J. Likelihood-enhanced fast translation functions. *Acta Crystallogr., Sect. D: Biol. Crystallogr.* **2005**, *61*, 458−464.
(72) Perrakis, A.; Morris, R.; Lamzin, V. S. Automated protein model building combined with iterative structure refinement. *Nat. Struct. Biol.* **1999**, *6*, 458−463.
(73) Emsley, P.; Cowtan, K. Coot: model-building tools for molecular graphics. *Acta Crystallogr., Sect. D: Biol. Crystallogr.* **2004**, *60*, 2126−2132.
(74) Murshudov, G. N.; Vagin, A. A.; Dodson, E. J. Refinement of macromolecular structures by the maximum-likelihood method. *Acta Crystallogr., Sect. D: Biol. Crystallogr.* **1997**, *53*, 240−255.
(75) Painter, J.; Merritt, E. A. Optimal description of a protein structure in terms of multiple groups undergoing TLS motion. *Acta Crystallogr., Sect. D: Biol. Crystallogr.* **2006**, *62*, 439−450.
(76) Filippakopoulos, P.; Picaud, S.; Fedorov, O.; Keller, M.; Wrobel, M.; Morgenstern, O.; Bracher, F.; Knapp, S. Benzodiazepines and benzotriazepines as protein interaction inhibitors targeting bromodomains of the BET family. *Bioorg. Med. Chem.* **2012**, *20*, 1878−1886.
(77) Picaud, S.; Wells, C.; Felletar, I.; Brotherton, D.; Martin, S.; Savitsky, P.; Diez-Dacal, B.; Philpott, M.; Bountra, C.; Lingard, H.; Fedorov, O.; Muller, S.; Brennan, P. E.; Knapp, S.; Filippakopoulos, P. RVX-208, an inhibitor of BET transcriptional regulators with selectivity for the second bromodomain. *Proc. Natl. Acad. Sci. U.S.A.* **2013**, *110*, 19754−19759.
(78) Ghosh, A. K.; Lagisetty, P.; Zajc, B. Direct synthesis of 8-fluoro purine nucleosides via metalation−fluorination. *J. Org. Chem.* **2007**, *72*, 8222−8226.
(79) Roy, A.; Schneller, S. W. An unusual occurrence on attempted purine C-8 electrophilic fluorination of 5′-noraristeromycin. *Org. Lett.* **2005**, *7*, 3889−3891.
(80) De, A.; Jasani, A.; Arora, R.; Gambhir, S. S. Evolution of BRET biosensors from live cell to tissue-scale in vivo imaging. *Front. Endocrinol. (Lausanne, Switz.)* **2013**, *4*, 131.

DOI: 10.1021/jm501893k
J. Med. Chem. 2015, 58, 2718−2736